



2 DOCTORAL THESIS

---

4 Optimisation studies and background  
5 estimation in searches for the supersymmetric  
6 partner of the top quark in all-hadronic final  
7 states with the ATLAS Detector at the LHC

---

9 *A thesis submitted in fulfillment of the requirements  
10 for the degree of Doctor of Philosophy*

11 *in the*

12 Experimental Particle Physics Research Group  
13 School of Mathematical and Physical Sciences

14 *Author:* **Fabrizio MIANO** *Supervisor:* **Dr. Fabrizio SALVATORE**

15 17th November 2017

Dedicated to my family.

*Have no fear for atomic energy  
'cause none of them can stop the  
time*

17

---

Robert Nesta Marley

18

## *Acknowledgments*

- 19 Thanks to every single thing that went wrong. It made me stronger.

## *Declaration*

21 I, Fabrizio MIANO, hereby declare that this thesis, titled, "Optimisation studies and back-  
22 ground estimation in searches for the supersymmetric partner of the top quark in all-  
23 hadronic final states with the ATLAS Detector at the LHC" has not been and will not be,  
24 submitted in whole or in part to another University for the award of any other degree.

25 *Brighton, 17th November 2017*

27                                  University of Sussex  
28                                  School of Mathematical and Physical Sciences  
29                                  Experimental Particle Physics Research Group

30                                  Doctoral Thesis

31                                  

---

  
32                                  Optimisation studies and background estimation in searches for  
33                                  the supersymmetric partner of the top quark in all-hadronic final  
34                                  states with the ATLAS Detector at the LHC  
35                                  

---

36                                  by Fabrizio MIANO

37                                  *Abstract*

38     This thesis presents searches for supersymmetry in  $\sqrt{s} = 13$  TeV proton-proton collisions  
39     at the LHC using data collected by the ATLAS detector in 2015, 2016 and 2017. Events  
40     with 4 or more jets and missing transverse energy were selected. Kinematic variables were  
41     investigated and optimisations were performed to increase the sensitivity to supersym-  
42     metric signals. Standard Model backgrounds were estimated by means of Monte Carlo  
43     simulations and data-driven techniques. Before analysing the data in the blinded signal  
44     regions the agreement between data and background predictions and the extrapolations  
45     from control and validation regions to signal regions were validated. The analysis yiel-  
46     ded no significant excess in any of the analyses performed. Therefore limits were set and  
47     the results were interpreted as lower bounds on the masses of supersymmetric particles  
48     in various scenarios and models.

# <sup>49</sup> Contents

<sup>50</sup>	<b>Introduction</b>	<b>1</b>
<sup>51</sup>	<b>1 The Standard Model of particle physics and Supersymmetry</b>	<b>2</b>
<sup>52</sup>	<b>1.1 The Standard Model</b> . . . . .	2
<sup>53</sup>	<b>1.1.1 Electroweak Symmetry Breaking and the Higgs mechanism</b> . . . . .	6
<sup>54</sup>	<b>1.1.2 Limitations of the Standard Model</b> . . . . .	9
<sup>55</sup>	<b>1.2 Supersymmetry</b> . . . . .	11
<sup>56</sup>	<b>1.2.1 Why SUSY?</b> . . . . .	11
<sup>57</sup>	<b>1.2.2 Minimal Supersymmetric Standard Model</b> . . . . .	12
<sup>58</sup>	<b>1.2.3 Phenomenology of Supersymmetry</b> . . . . .	15
<sup>59</sup>	<b>2 The ATLAS Experiment at the LHC</b>	<b>20</b>
<sup>60</sup>	<b>2.1 The LHC</b> . . . . .	20
<sup>61</sup>	<b>2.2 The ATLAS Detector</b> . . . . .	23
<sup>62</sup>	<b>2.2.1 The Magnet System</b> . . . . .	24
<sup>63</sup>	<b>2.2.2 The Inner Detector</b> . . . . .	25
<sup>64</sup>	<b>2.2.3 The Calorimeters</b> . . . . .	28
<sup>65</sup>	<b>2.2.4 The Muon Spectrometer</b> . . . . .	29
<sup>66</sup>	<b>2.3 The ATLAS Trigger System</b> . . . . .	30
<sup>67</sup>	<b>2.3.1 Level 1 Trigger</b> . . . . .	32
<sup>68</sup>	<b>2.3.2 High-Level Trigger</b> . . . . .	32
<sup>69</sup>	<b>3 The <i>b</i>-jet Trigger Signature in ATLAS</b>	<b>33</b>
<sup>70</sup>	<b>3.1 Trigger Efficiency</b> . . . . .	33
<sup>71</sup>	<b>4 Event Simulation and Reconstruction</b>	<b>34</b>
<sup>72</sup>	<b>4.1 Event Generation</b> . . . . .	34
<sup>73</sup>	<b>4.1.1 Parton Distribution Functions (PDFs)</b> . . . . .	34

74	4.1.2 Matrix Element Calculation . . . . .	34
75	4.1.3 Parton Showers . . . . .	34
76	4.1.4 Hadronisation . . . . .	34
77	4.2 Detector Simulation . . . . .	34
78	<b>5 Stop searches in final states with jets and missing transverse energy</b>	35
79	<b>6 Results and Statistical Intepretations</b>	36
80	<b>Trigger</b>	37
81	<b>Bibliography</b>	38

## <sup>82</sup> List of Tables

<sup>83</sup>	1.1 Forces and mediators described by the SM . . . . .	5
<sup>84</sup>	1.2 SUSY particles in the MSSM . . . . .	15
<sup>85</sup>	1.3 Parameters in the pMSSM. . . . .	17

# <sup>86</sup> List of Figures

<sup>87</sup> 1.1	The elementary particles of the Standard Model. From the outermost to the innermost; fermions (quarks, top-half wheel, leptons, bottom-half wheel), vector bosons, and the Higgs boson. . . . .	3
<sup>88</sup> 1.2	The Higgs potential in the complex plane. . . . .	8
<sup>89</sup> 1.3	Summary of several Standard Model total production cross-section measurements, corrected for leptonic branching fractions, compared to the corresponding theoretical expectations. All theoretical expectations were calculated at NLO or higher. The luminosity used for each measurement is indicated close to the data point. Uncertainties for the theoretical predictions are quoted from the original ATLAS papers. They were not always evaluated using the same prescriptions for PDFs and scales. Not all measurements are statistically significant yet [1]. . . . .	9
<sup>90</sup> 1.4	The inverse couplings of electromagnetic (dashed blue), weak (dashed red) and strong (solid green) interactions with the SM (left) and a supersymmetric model (right). In the SM the three lines do not meet at one point, but with the introduction of supersymmetry, and assuming that the supersymmetric particles are not heavier than about 1 TeV, they do meet. This is an indication that supersymmetry could be discovered at the LHC. . . . .	12
<sup>91</sup> 1.5	NLO+NLL production cross-sections as a function of mass at $\sqrt{s} = 13\text{TeV}$ [2]	18
<sup>92</sup> 1.6	Illustration of stop decay modes in the $(m_{\tilde{t}_1}, m_{\tilde{\chi}_1^0})$ mass place where the $\tilde{\chi}_1^0$ is assumed to be the lightest supersymmetric particle. The dashed blue lines indicate thresholds separating regions where different processes dominate.	19
<sup>93</sup> 1.7	Diagrams of the decay topologies of the signal models considered in this work. The term "soft" refers to decay products that have transverse momenta below the detector thresholds. . . . .	19

112	2.1 CERN Accelerator complex. The LHC is the last ring (dark grey line). Smaller machines are used for early-stage acceleration and also to provide beams for other experiments [3]. . . . .	22
115	2.2 Cut-away view of the ATLAS detector. The dimensions of the detector are 25 m in height and 44 m in length. The overall weight of the detector is approximately 7000 tonnes [3]. . . . .	23
118	2.3 The ATLAS magnet system. . . . .	25
119	2.4 The ATLAS Inner Detector . . . . .	26
120	2.5 A computer generated image of the full calorimeter. . . . .	28
121	2.6 Cut-away view of the ATLAS muon system [4]. . . . .	30
122	2.7 The ATLAS TDAQ system. L1Topo and FTK were being commissioned during 2015 and not used for the results shown in this thesis [5]. . . . .	31
123		

# <sup>124</sup> Introduction

<sup>125</sup> Last thing to write

<sup>126</sup> **1** | <sup>127</sup> **The Standard Model of particle physics and Supersymmetry**

<sup>128</sup>

*A theory is something nobody believes, except the person who made it. An experiment is something everybody believes, except the person who made it.*

---

Albert Einstein

<sup>129</sup> In this chapter, an overview of the Standard Model of particle physics will be presented in Section 1.1 together with its limitations in Section 1.1.2. After having discussed the <sup>130</sup> reasons behind the need of an extension, which theoretical physicists have been trying to <sup>131</sup> provide for the last decades, one of the most popular, Supersymmetry, will be discussed <sup>132</sup> in Section 1.2. Here, an overview of the theory together with the motivations behind its <sup>133</sup> success, will be presented in Section 1.2.1, followed by the description of the Minimal <sup>134</sup> Supersymmetric Standard Model (MSSM) in Section 1.2.2, and finally, the phenomenology <sup>135</sup> of Supersymmetry, with particular attention on third-generation Supersymmetry, as <sup>136</sup> it is the most relevant theoretical support to the analyses presented in this work, will be <sup>137</sup> discussed in Section 1.2.3.

<sup>139</sup> **1.1 The Standard Model**

<sup>140</sup> The SM is an effective theory that aims to provide a general description of fundamental <sup>141</sup> particles and the phenomena we see in nature, i. e. the way they interact. Unfortunately, <sup>142</sup> our understanding of nature is still limited due to some opened question the SM is not <sup>143</sup> able to answer to.

<sup>144</sup> The 20<sup>th</sup> century can be considered a quantum revolution. Several experiments led to <sup>145</sup> discoveries which were found to be, together with the formalised theory, a solid base of

<sup>146</sup> the Standard Model of particle physics and our description of nature. Several particles  
<sup>147</sup> were first predicted and then experimentally observed e. g. the  $W$  and the  $Z$  bosons, the  $\tau$   
<sup>148</sup> lepton, [6], and more recently the Higgs boson at the LHC discovered by ATLAS [7] and  
<sup>149</sup> CMS [8].

<sup>150</sup> The SM lays on a Quantum Field The-  
<sup>151</sup> ory (QFT) where particles are treated like  
<sup>152</sup> field excitations. It can describe three of  
<sup>153</sup> the four fundamental forces; weak, electro-  
<sup>154</sup> magnetic, and strong, but not gravity.

<sup>155</sup> The most general classification of the  
<sup>156</sup> elementary particles within the SM can be  
<sup>157</sup> made by means of spin. Fermions (leptons  
<sup>158</sup> and quarks), usually referred to as matter,  
<sup>159</sup> which have half-integer spin values, and  
<sup>160</sup> bosons, usually referred to as information  
<sup>161</sup> carriers, which have integer-spin values. A  
<sup>162</sup> noteworthy subset of bosons is formed by  
<sup>163</sup> the Spin-1 bosons, also known as gauge  
<sup>164</sup> bosons. These can be considered medi-  
<sup>165</sup> ators of the forces. Figure 1.1 displays  
<sup>166</sup> the elementary particles of the Standard  
<sup>167</sup> Model known as of today.

## <sup>168</sup> Fermions

<sup>169</sup> Six quarks and six leptons belong to the fermions family. In particular, fermions can be  
<sup>170</sup> grouped into three generations. Each generation contains four particles; one up- and one  
<sup>171</sup> down-type quark, one charged lepton and one neutral lepton. The masses of the charged  
<sup>172</sup> leptons and quarks increase with the generation. The six quarks of the SM can be grouped  
<sup>173</sup> into three doublets;

$$\begin{pmatrix} u \\ d \end{pmatrix}, \quad \begin{pmatrix} c \\ s \end{pmatrix}, \quad \begin{pmatrix} t \\ b \end{pmatrix}$$

<sup>174</sup> The up-type quarks (*up, charm, top*) have charge  $+\frac{2}{3}e$  and the down-type quarks (*down,*  
<sup>175</sup> *strange, beauty/bottom*) have charge  $-\frac{1}{3}e$ , where  $e$  is the electron charge. Quarks also have

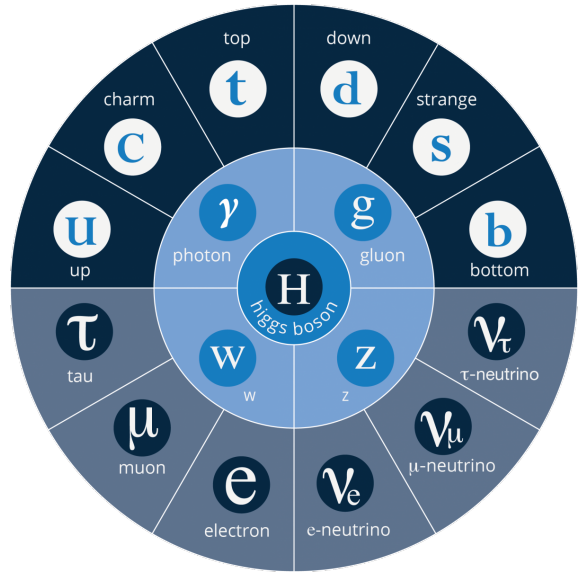


Figure 1.1: The elementary particles of the Standard Model. From the outermost to the innermost; fermions (quarks, top-half wheel, leptons, bottom-half wheel), vector bosons, and the Higgs boson.

<sup>176</sup> another quantum number that can be seen as the analogue of the electric charge; the col-  
<sup>177</sup> our charge. This can exist in three different states; *red*, *green* and *blue*. Moreover, as a con-  
<sup>178</sup> sequence of *confinement*, which will be discussed later on in this section, quarks cannot  
<sup>179</sup> exist as free particles. They rather group to form hadronic matter, also known as *had-*  
<sup>180</sup> *rons*. There are two kinds of hadrons; mesons and baryons. Mesons are quark-antiquark  
<sup>181</sup> systems, e.g. the pion, and baryons are three-quark system, e.g. protons and neutrons.  
<sup>182</sup> Quarks and anti-quarks have a baryon number of  $\frac{1}{3}$  and  $-\frac{1}{3}$ , respectively.

<sup>183</sup> There are six leptons and they can be classified in charged leptons (electron  $e^-$ , muon  
<sup>184</sup>  $\mu^-$ , tau  $\tau^-$ ) and neutral leptons (electron neutrino  $\nu_e$ , muon neutrino  $\nu_\mu$ , tau neutrino  $\nu_\tau$ ).

$$\begin{pmatrix} \nu_e \\ e^- \end{pmatrix}, \quad \begin{pmatrix} \nu_\mu \\ \mu^- \end{pmatrix}, \quad \begin{pmatrix} \nu_\tau \\ \tau^- \end{pmatrix}$$

<sup>185</sup> Each lepton has a characteristic quantum number, called lepton number ( $L$ ). Negatively  
<sup>186</sup> (positively) charged leptons have  $L = -1$  ( $L = 1$ ) and neutral leptons have  $L = 0$ . The  
<sup>187</sup> lepton number is conserved in all the interactions.

## <sup>188</sup> Forces of Nature

<sup>189</sup> Forces in the SM are described by gauge theories, where the interactions is mediated by  
<sup>190</sup> a vector gauge boson.

<sup>191</sup> The electromagnetic force is described by Quantum ElectroDynamics (QED) and, as  
<sup>192</sup> its mediator is the photon ( $\gamma$ ) which couples to charged particles, it only affects charged  
<sup>193</sup> leptons and quarks, not neutrinos which are instead affected by the weak force, mediated  
<sup>194</sup> by the  $W^\pm$  and  $Z^0$  bosons.

<sup>195</sup> The weak interaction is associated with handedness (the projection of a particle spin  
<sup>196</sup> onto its direction of motion). Both leptons and quarks have left- and right-handed com-  
<sup>197</sup> ponents. However, only the left-handed (right-handed) component for neutrinos (anti-  
<sup>198</sup> neutrinos) has been observed. This means that nature prefers to produce left-handed  
<sup>199</sup> neutrinos and right-handed anti-neutrinos, which is the so-called *parity violation*.

<sup>200</sup> The strong interaction, mediated by the gluon, electrically neutral and massless, is  
<sup>201</sup> described by Quantum ChromoDynamics (QCD). Its coupling increases with increasing  
<sup>202</sup> distance and is smaller at short range. Moreover, due to gluon self interactions, which  
<sup>203</sup> will be discussed in the next paragraph, two different phenomena arise;

- <sup>204</sup> • *confinement*: quarks or gluons cannot be observed as free particles, but only col-  
<sup>205</sup> ourless “singlet” states can be observed as “jets”, namely collimated cone-shaped

206 sprays of hadrons;

- 207 • *asymptotic freedom*: interactions between quarks and gluons become weaker as the  
208 energy scale increases and the corresponding length scale decreases

209 Table 1.1 summarises the forces described in the SM and the main characteristics of  
210 the mediators. The gravitational force is believed to be mediated by the graviton, but as  
211 already mentioned, since it is not included in the SM, it will not be further discussed.

Table 1.1: Forces and mediators described by the SM

Force	Name	Symbol	Mass [GeV]	Charge
Electromagnetic	Photon	$\gamma$	0	0
Weak	W	$W^\pm$	80.398	$\pm e$
	Z	$Z^0$	91.188	0
Strong	Gluon	$g$	0	0

## 212 Symmetries and Gauge Groups

213 In 1915, the German mathematician and theoretical physicist Emmy Noether (23 March  
214 1882 – 14 April 1935) proved that every differentiable symmetry of the action - defined  
215 as the integral over space of a Lagrangian density function - of a physical system has a  
216 corresponding conservation law. More generally, a symmetry is a property of a physical  
217 system and under certain transformations this property is preserved.

218 A gauge theory in QFT, is a theory in which the Lagrangian is invariant under a con-  
219 tinuous group of local transformation. Group theory was adopted to describe the sym-  
220 metries conserved in the SM. The gauge group of the SM is the *Lie Group* which contains  
221 all the transformations between possible gauges. The Lie algebra of group generators is  
222 associated to any Lie group and for each group generator there emerges a corresponding  
223 field, called the gauge field, and the quanta of such fields are called *gauge bosons*.

224 The three SM interactions can therefore be mathematically described by the following:

$$U(1)_Y \otimes SU(2)_L \otimes SU(3)_C \quad (1.1)$$

225 Here,  $Y$  is the weak hypercharge, used to estimate the correlation between the electric  
226 charge ( $Q$ ) and the third component of the weak isospin ( $I_3$ ) via the relation  $Q = I_3 + Y/2$ ,  
227 where  $I_3$  can either be  $\pm 1/2$  or 0 for left-handed and right-handed particles, respectively;  
228  $C$  the colour charge and  $L$  the left-handedness.

<sup>229</sup> As of today, three of the four known forces of nature can be described using group  
<sup>230</sup> theory.

<sup>231</sup> QED is an Abelian gauge theory described by the symmetry group  $U(1)$ . The electro-  
<sup>232</sup> magnetic four-potential is its gauge field and the photon its gauge boson [9]. The interac-  
<sup>233</sup> tions between charged fermions occurs by the exchange of a massless photon.

<sup>234</sup> The weak interaction is described by the non-Abelian gauge group  $SU(2)$ . The  $SU(2)$   
<sup>235</sup> generators are the massless gauge bosons  $W_\mu^{\alpha=1,\dots,3}$  and, as mentioned earlier on in this  
<sup>236</sup> chapter, they violate the parity by acting only on left-handed particles. As a consequence  
<sup>237</sup> of non-Abelianity,  $SU(2)$  gauge bosons can self-interact as the generator commutators  
<sup>238</sup> are non-vanishing. Additionally, quarks can also interact through weak interaction as  
<sup>239</sup> mixtures of SM eigenstates as described by the CKM matrix [10].

<sup>240</sup> Finally, the strong interaction, described by the symmetry group  $SU(3)$ , has eight  
<sup>241</sup> massless gauge bosons, the gluons,  $G_\mu^{\alpha=1,\dots,8}$  which can be exchanged between quarks  
<sup>242</sup> and can also self-interact.

### <sup>243</sup> 1.1.1 Electroweak Symmetry Breaking and the Higgs mechanism

<sup>244</sup> In 1979 Sheldon Glashow, Abdus Salam, and Steven Weinberg were awarded the Nobel  
<sup>245</sup> Prize in Physics for their contributions to the so-called electroweak unification. In the  
<sup>246</sup> mathematical description of the SM in 1.1, the electroweak interaction is described by  
<sup>247</sup>  $U(1)_Y \otimes SU(2)_L$ .

<sup>248</sup> The four electroweak physical bosons  $W^\pm$ ,  $Z$  and  $\gamma$  are related to the four unphysical  
<sup>249</sup> gauge bosons  $W_\mu^{\alpha=1,\dots,3}$  and  $B_\mu$ . In particular, to obtain the physical bosons the gauge  
<sup>250</sup> bosons have to mix as follows;

$$\begin{pmatrix} A_\mu \\ Z_\mu \end{pmatrix} = \begin{pmatrix} \cos \theta_W & \sin \theta_W \\ -\sin \theta_W & \cos \theta_W \end{pmatrix} \begin{pmatrix} B_\mu \\ W_\mu^3 \end{pmatrix} \quad (1.2)$$

<sup>251</sup> Here,  $\theta_W$  is the so-called *Weinberg angle* which is the angle by which spontaneous sym-  
<sup>252</sup> metry breaking rotates the original gauge bosons  $W_\mu^3$  and  $B_\mu$  into the physical  $Z$  and  $\gamma$ .  
<sup>253</sup>  $A_\mu$  and  $Z_\mu$  represent the photon and the  $Z$  boson, respectively. The  $\theta_W$  angle can be ex-  
<sup>254</sup> perimentally determined in terms of the coupling strengths, of the  $B_\mu(g_1)$  and the  $W_\mu^\alpha(g_2)$   
<sup>255</sup> to the fermions, using the relation  $\tan \theta_W = g_1/g_2$ . The field mixing of gauge bosons that  
<sup>256</sup> gives birth to the physical ones can be mathematically expressed by the following:

$$A_\mu = W_\mu^3 \sin \theta_W + B_\mu \cos \theta_W \quad (1.3)$$

257

$$Z_\mu = W_\mu^3 \cos \theta_W - B_\mu \sin \theta_W \quad (1.4)$$

258 and the two charged  $W$  bosons are defined as;

$$W_\mu^\pm = \frac{1}{\sqrt{2}} (W_\mu^1 \mp i W_\mu^2) \quad (1.5)$$

259 The mass terms for both gauge bosons and fermionic fields are forbidden by the elec-  
 260 troweak gauge as they are not invariant under gauge transformations. Nonetheless, it was  
 261 experimentally proven that  $W$  and  $Z$  bosons are massive [9], therefore in order for the SM  
 262 assumption to hold, the electroweak symmetry must be broken.

263 The SM Lagrangian can be written as the sum of the various Lagrangians describing  
 264 the three interactions and the masses of the elementary particles as follows:

$$\mathcal{L}_{\text{SM}} = \mathcal{L}_{\text{EWK}} + \mathcal{L}_{\text{QCD}} + \mathcal{L}_{\text{Mass}} \quad (1.6)$$

265 In order for the SM Lagrangian to remain a renormalisable theory, the mass terms ( $\mathcal{L}_{\text{Mass}}$ )  
 266 cannot be inserted by hand. A mechanism, that can preserve the gauge symmetry in the  
 267 SM and can solve the inconsistency arisen from the mass difference between the gauge  
 268 bosons and the physical ones, is needed. A British theoretical physicist, Peter Higgs (29  
 269 May 1929, Newcastle upon Tyne, UK), came up with a brilliant solution for which he was  
 270 awarded the Nobel Prize in Physics in 2013. Higgs proposed that broken symmetry in  
 271 the electroweak theory could explain the origin of masses of elementary particles, and  
 272 in particular of  $W$  and  $Z$  bosons. It was around 1960's when the Higgs mechanism was  
 273 about to be given birth. The mechanism introduces a scalar field, known as the Higgs  
 274 field, thought to couple to both massive fermions and bosons. The  $SU(2)$  doublet is then  
 275 introduced in the SM;

$$\phi = \begin{pmatrix} \phi^+ \\ \phi^0 \end{pmatrix} \quad (1.7)$$

276 with  $\phi^+$  and  $\phi^0$  generic complex fields:

$$\phi^+ = \frac{\phi_1 + i\phi_2}{\sqrt{2}}, \quad \phi^0 = \frac{\phi_3 + i\phi_4}{\sqrt{2}} \quad (1.8)$$

277 Consider a Lagrangian of the form:

$$\mathcal{L}_{\text{Higgs}} = (\partial_\mu \phi)^* (\partial^\mu \phi) - V(\phi) \quad (1.9)$$

<sup>278</sup> Renormalizability and  $SU(2)_L \otimes U(1)_Y$  invariance require the Higgs potential to be of the  
<sup>279</sup> following form:

$$V(\phi) = \mu^2 \phi^\dagger \phi + \lambda (\phi^\dagger \phi)^2 \quad (1.10)$$

<sup>280</sup> The Lagrangian in Eq. 1.9 is the Higgs Lagrangian if  $\phi$  is chosen to be the following:

$$\phi = \begin{pmatrix} \phi^+ \\ \phi^0 \end{pmatrix} = \begin{pmatrix} G^+ \\ \frac{1}{\sqrt{2}}(v + H + iG^0) \end{pmatrix}$$

<sup>281</sup> Here, the complex scalar field  $G^\pm$  and the real scalar field  $G^0$  correspond to Goldstone  
<sup>282</sup> bosons, and the real scalar field  $H$  is the SM Higgs boson field [11]. These massless scalars  
<sup>283</sup> are absorbed due to the gauge transformations by the electroweak gauge bosons of the SM:

$$\phi = \begin{pmatrix} \phi^+ \\ \phi^0 \end{pmatrix} = \begin{pmatrix} 0 \\ \frac{1}{\sqrt{2}}(v + H) \end{pmatrix} \quad (1.11)$$

<sup>284</sup> The Higgs potential in Eq. 1.10 is displayed in Fig. 1.2 if  $\lambda$  and  $\mu$  are chosen to be real.  
<sup>285</sup> Such potential has a non-zero ground state,  $v$ , also known as *vacuum expectation value*  
<sup>286</sup> (VEV):

$$\phi_0 = \begin{pmatrix} 0 \\ \frac{1}{\sqrt{2}}v \end{pmatrix} \quad (1.12)$$

<sup>287</sup> Such representation remains invariant under  $U(1)$  allowing electric charge conservation.  
<sup>288</sup> However, the SM gauge symmetry 1.1 is broken into  $SU(2)_L \otimes U(1)_Y$ .

<sup>289</sup>

In summary, to generate particle masses

<sup>290</sup>

gauge symmetry must be broken. However, in order for the theory to remain renormalisable, the global Lagrangian symmetry must be preserved. This can be solved introducing the concept of *spontaneous symmetry breaking* (SSB): a mechanism that allows a symmetric Lagrangian, but not a symmetric VEV. In particular,

<sup>291</sup>

<sup>292</sup>

<sup>293</sup>

<sup>294</sup>

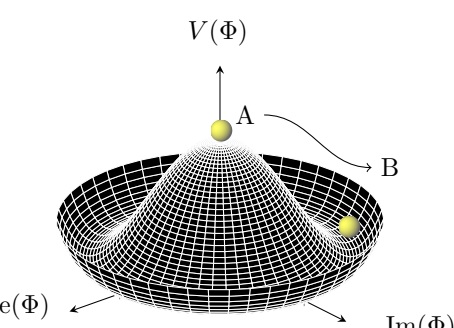
<sup>295</sup>

<sup>296</sup>

<sup>297</sup>

<sup>298</sup> Figure 1.2: The Higgs potential in the complex plane.

<sup>299</sup>



given a Lagrangian invariant under a certain transformation,  $T_X$ , and a generic set

of states, that transform under  $T_X$  as the elements of a multiplet, the symmetry is spontaneously broken if one of those states is arbitrarily chosen as the ground state of the system. The interaction of the Higgs field with the  $SU(2) \otimes U(1)$  gauge fields,  $W_\mu^{\alpha=1,2,3}$ , result in the three gauge bosons fields acquiring mass whilst the  $B_\mu$  field remains massless.

### 1.1.2 Limitations of the Standard Model

During Run 1 and 2 of the LHC, the SM has been extensively validated, as shown in Fig. 1.3: the agreement, between the measured production cross-section of various SM processes and the SM predictions, looks very good. However, the reasons behind the mass difference between the three generations of fermions are still not explained by the SM, since masses are treated as free parameters in the theory. In addition, there are some fundamental questions that have still no answer and they will be briefly discussed this section.

**Standard Model Total Production Cross Section Measurements** Status: July 2017

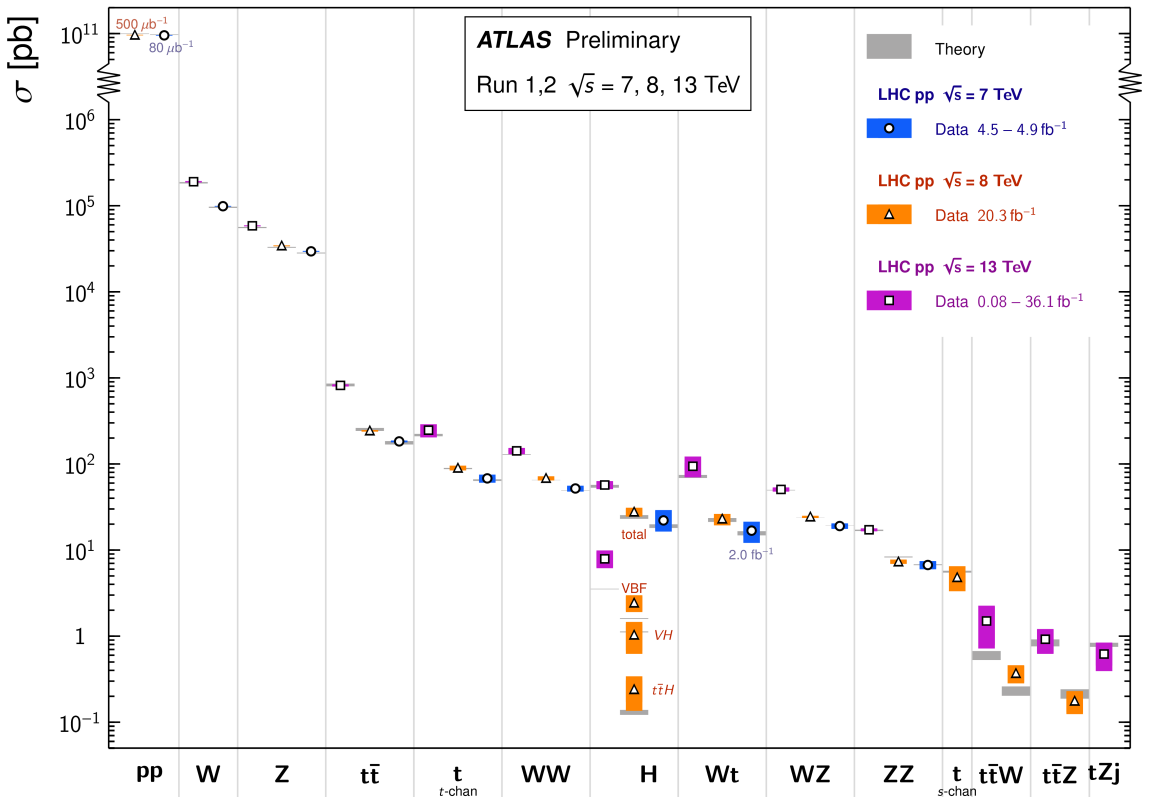


Figure 1.3: Summary of several Standard Model total production cross-section measurements, corrected for leptonic branching fractions, compared to the corresponding theoretical expectations. All theoretical expectations were calculated at NLO or higher. The luminosity used for each measurement is indicated close to the data point. Uncertainties for the theoretical predictions are quoted from the original ATLAS papers. They were not always evaluated using the same prescriptions for PDFs and scales. Not all measurements are statistically significant yet [1].

**312 Hierarchy Problem**

**313** Due to the coupling of the Higgs field to the fermionic fields the one-loop corrections to  
**314** the Higgs mass receive several contributions. In particular:

$$\Delta m_H^2 = -\frac{|\lambda_f|^2}{8\pi^2} \Lambda_{\text{UV}}^2 + \dots \quad (1.13)$$

**315** where,  $\lambda_f$  is the coupling constant to the fermionic field;  $\Delta m_H^2$  is the difference between  
**316** the observed Higgs mass  $m_H^2$  and the bare mass,  $m_H^0$  (Lagrangian parameter);  $\Lambda_{\text{UV}}$  is  
**317** the ultraviolet momentum cut-off, selected to be at the Planck scale ( $\sim 2 \cdot 10^{18}$  GeV), at  
**318** which a QFT description of gravity is believed to become possible. The correction to the  
**319** Higgs mass then, will be around 30 orders of magnitude larger than Higgs mass itself,  
**320** in opposition to what has been measured. This difference just mentioned, between the  
**321** electroweak scale and the Planck scale arisen from the quantum corrections to the Higgs  
**322** mass, is the so-called Hierarchy Problem [12].

**323 Neutrino Masses**

**324** The Super-Kamiokande Collaboration first, in 1998 [13], and SNO Collaboration later, in  
**325** 2001 [14], have provided measurements of the neutrino flux from solar and atmospheric  
**326** sources. The Nobel Prize in Physics 2015 was awarded jointly to Takaaki Kajita and Arthur  
**327** B. McDonald “for the discovery of neutrino oscillations, which shows that neutrinos have  
**328** mass” [15]. Such feature contradicts the absence of a mechanism for mass generation for  
**329** the neutrinos.

**330 Dark Matter**

**331** Although dark matter (DM) has never been directly observed, its existence is inferred from  
**332** its gravitational effects. For example, looking at galaxies rotation, it was observed that the  
**333** rotation speed was higher than expected, given the amount of visible matter. Two differ-  
**334** ent reasoning arose during the last century to justify such effect: there is either matter that  
**335** cannot be seen by us (in terms of visible light), which contributes to the galactic mass, or  
**336** the general relativity works differently at galactic distances. The former is believed to  
**337** be the most likely and it implies the existence of new particles which do not interact via  
**338** electromagnetic interaction, the so-called Weakly Interacting Massive Particles (WIMPs).

## <sup>339</sup> 1.2 Supersymmetry

<sup>340</sup> Supersymmetry, also known as SUSY, introduces a space-time symmetry that relates bo-  
<sup>341</sup> sons to fermions and vice-versa, via a transformation of the form of:

$$Q |\text{fermion}\rangle = |\text{boson}\rangle, \quad Q |\text{boson}\rangle = |\text{fermion}\rangle \quad (1.14)$$

<sup>342</sup> For each SM particle there exists a supersymmetric partner, generally called *sparticle* (where  
<sup>343</sup> the s stands for “scalar”), with a spin difference of  $\Delta s = 1/2$ . Each pair of partners is ar-  
<sup>344</sup> ranged in a so-called *supermultiplet*. The two components have same masses and quantum  
<sup>345</sup> numbers, but different spin. *Sleptons* and *squarks* gauge mechanism is the same as their SM  
<sup>346</sup> equivalent, namely for example, the superpartners of the left-handed SM fermion com-  
<sup>347</sup> ponents couple weakly, but the superpartners of the right-handed SM fermion com-  
<sup>348</sup> ponents do not. Furthermore, gauge supermultiplets contain a vector boson and two spin-  
<sup>349</sup>  $\frac{1}{2}$  fermions. Spin-1 bosons are arranged in gauge multiplets, and their superpartners,  
<sup>350</sup> referred to as *gauginos*, are spin- $\frac{1}{2}$  fermions. Differently from the SM, the Spin-0 Higgs  
<sup>351</sup> boson has two supermultiplets containing sparticles with different weak isospin values,  
<sup>352</sup> referred to as  $H_u$  and  $H_d$ , which are required to give mass to both the up- and down-type  
<sup>353</sup> sparticles. Higgs SUSY partners are called the *Higgsinos*.

<sup>354</sup> As of today, SUSY particles have not been observed, resulting in the assumption that  
<sup>355</sup> SUSY must be a broken symmetry, otherwise superpartners would have the same quantum  
<sup>356</sup> numbers and masses as their SM equivalent. However, if sparticles were to be too heavy  
<sup>357</sup> (close to the Planck scale), the hierarchy problem would still remain unsolved. The *soft*  
<sup>358</sup> SUSY breaking mechanism, described in Section 1.2.2, overcomes this problem by impos-  
<sup>359</sup> ing constraints on the masses of sparticles to a range that can be experimentally explored.

### <sup>360</sup> 1.2.1 Why SUSY?

<sup>361</sup> One of the main motivations for SUSY is the cancellation of quadratic divergences to  
<sup>362</sup>  $\Delta m_H^2$ . The introduction of SUSY particles, with a half-integer spin difference with re-  
<sup>363</sup> spect to their SM partners, provides a solution to the hierarchy problem. The Higgs mass  
<sup>364</sup> squared potential receives corrections from a new scalar of mass  $m_S$  of the form:

$$\Delta m_H^2 = -\frac{|\lambda_S|^2}{16\pi^2} \left[ \Lambda_{\text{UV}}^2 - 2m_S^2 \ln(\Lambda_{\text{UV}}/m_S) + \dots \right] \quad (1.15)$$

<sup>365</sup> where,  $\lambda_S$  is the coupling of SUSY particles to the Higgs field. This term cancels the  
<sup>366</sup> fermionic contributions in Eq. 1.13 since the couplings are the same. The experimental

367 value of Higgs mass will then not need any fine tuning.

368 Furthermore, Fig. 1.4 shows the inverse couplings as a function of the scale for both SM  
369 and the Minimal Supersymmetric Standard Model (MSSM), which will be soon discussed.  
370 In the SM the three lines, representing electromagnetic (dashed blue), weak (dashed red)  
371 and strong (solid green) interactions respectively, do not meet at one point, but with the  
372 introduction of supersymmetry, and assuming that the supersymmetric particles are not  
373 heavier than about 1 TeV, they do meet. This is an indication that supersymmetry could  
374 be discovered at the LHC as well as another good motivation for SUSY searches given the  
375 possible unification of the coupling constants at the Planck scale.

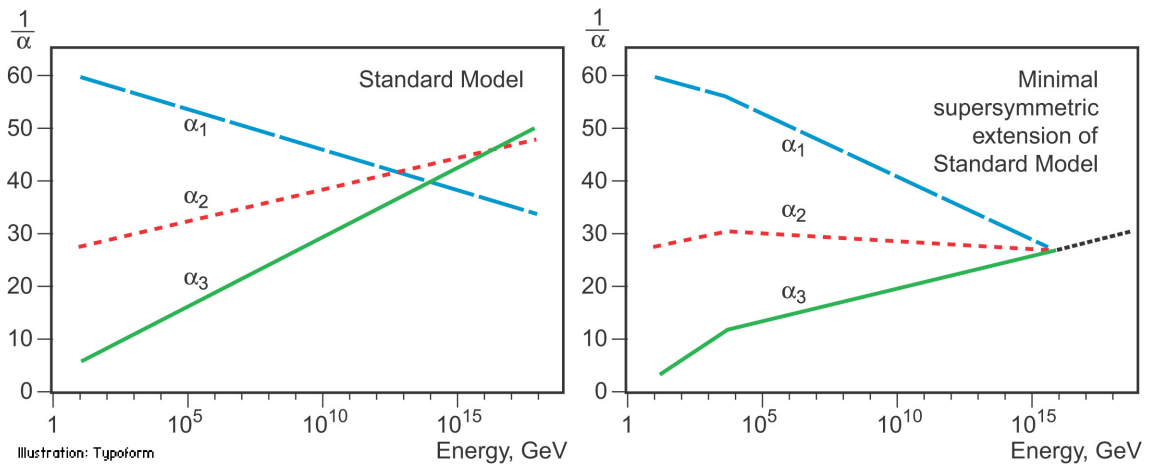


Figure 1.4: The inverse couplings of electromagnetic (dashed blue), weak (dashed red) and strong (solid green) interactions with the SM (left) and a supersymmetric model (right). In the SM the three lines do not meet at one point, but with the introduction of supersymmetry, and assuming that the supersymmetric particles are not heavier than about 1 TeV, they do meet. This is an indication that supersymmetry could be discovered at the LHC.

### 376 1.2.2 Minimal Supersymmetric Standard Model

377 There does not exist a unique extension of a supersymmetric Standard Model, i. e. SUSY  
378 is not a well-defined model but it is more a framework within which various SM exten-  
379 sions can be derived. The Minimal Supersymmetric Standard Model (MSSM), a minimal  
380 supersymmetric extension of the SM [16], is defined by essentially doubling up the num-  
381 ber of particles in the SM theory in order to include all the SM particles as well as their  
382 corresponding superpartners.

**383 Soft SUSY breaking**

384 The mass spectrum of the SUSY particles must sit somewhere at a larger scale than the SM  
 385 one, as supersymmetric particles have not been discovered at the mass scale of their SM  
 386 partners. This gives us a hint that supersymmetry cannot be an exact symmetry, there has  
 387 to be an analogous to the electroweak symmetry breaking discussed in 1.1.1 that breaks  
 388 SUSY. In particular, this must be soft or spontaneous such that broken supersymmetry  
 389 still provides a solution to the hierarchy problem. This means that some new higher-  
 390 energy-scale particles and interactions have to be added to the MSSM, but it also means  
 391 that terms, containing only masses and couplings, with positive mass dimension, gauge  
 392 invariant and violating SUSY, have to be added to the Lagrangian;

$$\mathcal{L}_{\text{MSSM}} = \mathcal{L}_{\text{SUSY}} + \mathcal{L}_{\text{soft}} \quad (1.16)$$

393 Here,  $\mathcal{L}_{\text{SUSY}}$  contains the original SUSY invariant interaction and  $\mathcal{L}_{\text{soft}}$  contains all the  
 394 additional terms. A set of around 100 parameters - depending on the method - are then  
 395 introduced into the theory.

396 A large amount of theoretical effort has been spent trying to understand the mech-  
 397 anism for soft SUSY breaking in order to produce the desired superpartner masses and  
 398 interactions properties. Among these three most studied mechanisms are;

- 399 • gravity-mediated supersymmetry breaking, also known as mSUGRA (minimal su-  
 400 pergravity), which communicates supersymmetry breaking to the supersymmetric  
 401 Standard Model through gravitational interactions [17];
- 402 • gauge-mediated supersymmetry breaking (GMSB) which communicates supersym-  
 403 metry breaking to the supersymmetric Standard Model through the Standard Model's  
 404 gauge interactions [18];
- 405 • anomaly-mediated supersymmetry breaking (AMSB), a special type of gravity-mediated  
 406 supersymmetry breaking, that communicates supersymmetry breaking to the su-  
 407 persymmetric Standard Model through the conformal anomaly [19, 20]

408 However, such models will not be discussed any further.

**409 MSSM mass spectrum**

410 As per the SM gauge bosons, the gaugino masses are affected by electroweak symmetry  
 411 breaking. The new mass terms, introduced in the  $\mathcal{L}_{\text{soft}}$ , mix to form the mass eigenstates

<sup>412</sup> of the sparticles. The neutral Winos,  $\tilde{W}^0$ , Binos,  $\tilde{B}^0$  and higgsinos  $\tilde{H}^0$  mix to form the four  
<sup>413</sup> *neutralinos*  $\tilde{\chi}_i^0$  ( $i = 1, 2, 3, 4$ ) as it follows;

$$\begin{pmatrix} \tilde{\chi}_1^0 \\ \tilde{\chi}_2^0 \\ \tilde{\chi}_3^0 \\ \tilde{\chi}_4^0 \end{pmatrix} = \begin{pmatrix} M_1 & 0 & -c_\beta s_W m_Z & c_W s_\beta m_Z \\ 0 & M_2 & c_\beta c_W m_Z & -c_W s_\beta m_Z \\ -c_\beta s_W m_Z & c_\beta s_W m_Z & 0 & -\mu \\ s_\beta c_W m_Z & -s_\beta c_W m_Z & -\mu & 0 \end{pmatrix} \begin{pmatrix} \tilde{B}^0 \\ \tilde{W}^0 \\ \tilde{H}_u^0 \\ \tilde{H}_d^0 \end{pmatrix} \quad (1.17)$$

<sup>414</sup> Here,  $c_\beta = \cos \beta$ ,  $(s_\beta) = \sin \beta$ ,  $c_W = \cos \theta_W$  and  $(s_W) = \sin \theta_W$ .  $M_1$ ,  $M_2$  are related  
<sup>415</sup> to gaugino masses and  $\mu$  to higgsino mass,  $\beta$  is the ratio of the electroweak coupling  
<sup>416</sup> constants and  $\theta_W$  is the ratio of the VEVs of the two Higgs doublet fields, and finally,  $m_Z$   
<sup>417</sup> ( $m_W$ ) is the mass of the  $Z$  ( $W$ ) boson. The neutralino indeces are conventionally assumed  
<sup>418</sup> to increase with their masses. The charged winos  $\tilde{W}^\pm$  and higgsinos  $\tilde{H}^\pm$  mix to form four  
<sup>419</sup> *charginos*,  $\tilde{\chi}_i^\pm$  ( $i = 1, 2$ ) as it follows;

$$\begin{pmatrix} \tilde{\chi}_1^\pm \\ \tilde{\chi}_2^\pm \end{pmatrix} = \begin{pmatrix} M_2 & \sqrt{2}m_W s_\beta \\ \sqrt{2}m_W c_\beta & \mu \end{pmatrix} \begin{pmatrix} \tilde{W}^\pm \\ \tilde{H}^\pm \end{pmatrix} \quad (1.18)$$

<sup>420</sup> Charginos and neutralinos, given birth by the mixing described in Eq. 1.18 and 1.17,  
<sup>421</sup> will be referred to as bino-like, wino-like or higgsino-like depending on their phenomenology.  
<sup>422</sup> Gluinos do not mix as they carry colour charge.

<sup>423</sup> The Higgs sector is also affected. There are five mass eigenstates,  $h^0$ ,  $H^0$ ,  $A^0$ , and  $H^\pm$ .  
<sup>424</sup> These, together with the other MSSM particles are listed in Table 1.2.

<sup>425</sup> In the MSSM the squark sector is specified by the mass matrix in the basis  $(\tilde{q}_L, \tilde{q}_R)$  with  
<sup>426</sup>  $\tilde{q} = \tilde{t}$  or  $\tilde{b}$  [21]. Left- and right-handed squarks and sleptons do not have to have equal  
<sup>427</sup> mass, which means that a rotation matrix can be defined, although the mixing is assumed  
<sup>428</sup> to be non-zero only for the third-generation scalar partners. Stop,  $\tilde{t}_L$ ,  $\tilde{t}_R$ , sbottom  $\tilde{b}_L$ ,  $\tilde{b}_R$ ,  
<sup>429</sup> and stau,  $\tilde{\tau}_L$ ,  $\tilde{\tau}_R$  rotate into mass eigenstates,  $\tilde{t}_1$ ,  $\tilde{t}_2$ ,  $\tilde{b}_1$ ,  $\tilde{b}_2$ ,  $\tilde{\tau}_1$ ,  $\tilde{\tau}_2$ , respectively, as described  
<sup>430</sup> in Eq. 1.19 [22].

$$\mathcal{M}_q^2 = \begin{pmatrix} m_{\tilde{q}_L}^2 & a_q m_q \\ a_q m_q & m_{\tilde{q}_R}^2 \end{pmatrix} \quad (1.19)$$

<sup>431</sup> with

Table 1.2: SUSY particles in the MSSM

Name	Spin	Gauge Eigenstates	Mass Eigenstates
Squarks ( $\tilde{q}$ )	0	$\tilde{u}_L \tilde{u}_R \tilde{d}_L \tilde{d}_R$	(same)
		$\tilde{c}_L \tilde{c}_R \tilde{s}_L \tilde{s}_R$	(same)
		$\tilde{t}_L \tilde{t}_R \tilde{b}_L \tilde{b}_R$	$\tilde{t}_1 \tilde{t}_2 \tilde{b}_1 \tilde{b}_2$
Sleptons ( $\tilde{l}$ )	0	$\tilde{e}_L \tilde{e}_R \tilde{\nu}_L$	(same)
		$\tilde{\mu}_L \tilde{\mu}_R \tilde{\nu}_L$	(same)
		$\tilde{\tau}_L \tilde{\tau}_R \tilde{\nu}_{\tau}$	$\tilde{\tau}_1 \tilde{\tau}_2 \tilde{\nu}_{\tau}$
Higgs bosons	0	$H_u^0 H_d^0 H_u^+ H_d^-$	$h^0 H^0 A^0 H^{\pm}$
Neutralinos ( $\tilde{\chi}_j^0$ )	1/2	$\tilde{B}^0 \tilde{W}^0 \tilde{H}_u^0 \tilde{H}_d^0$	$\tilde{\chi}_1^0 \tilde{\chi}_2^0 \tilde{\chi}_3^0 \tilde{\chi}_4^0$
Charginos ( $\tilde{\chi}_i^{\pm}$ )	1/2	$\tilde{W}^{\pm} \tilde{H}_u^{\pm} \tilde{H}_d^{\mp}$	$\tilde{\chi}_1^{\pm} \tilde{\chi}_2^{\pm}$
Gluino	1/2	$\tilde{g}$	(same)
Gravitino	3/2	$\tilde{G}$	(same)

$$\begin{aligned}
m_{\tilde{q}_L}^2 &= M_{\tilde{Q}}^2 + m_Z^2 \cos 2\beta \left( I_3^{qL} - e_q \sin^2 \theta_W \right) + m_q^2, \\
m_{\tilde{q}_R}^2 &= M_{\{\tilde{U}, \tilde{D}\}}^2 + m_Z^2 \cos 2\beta e_q \sin^2 \theta_W + m_q^2, \\
a_q m_q &= \begin{cases} (A_t - \mu \cot \beta) m_t, (\tilde{q} = \tilde{t}) \\ (A_b - \mu \tan \beta) m_t, (\tilde{q} = \tilde{b}) \end{cases}
\end{aligned} \tag{1.20}$$

432 Here,  $I_3^{qL}$  is the third component of the weak isospin and  $e_q$  the electric charge of the  
433 quark  $q$ .  $M_{\{\tilde{Q}, \tilde{U}, \tilde{D}\}}$  and  $A_{t,b}$  are soft SUSY-breaking parameters,  $\mu$  is the higgsino mass  
434 parameter, and  $\tan \beta$  is the ratio of Higgs field VEVs. By diagonalising the matrix in  
435 Eq. 1.19 one gets the mass eigenstates

$$\tilde{q}_1 = \tilde{q}_L \cos \theta_{\tilde{q}} + \tilde{q}_R \sin \theta_{\tilde{q}}$$

$$\tilde{q}_2 = -\tilde{q}_L \sin \theta_{\tilde{q}} + \tilde{q}_R \cos \theta_{\tilde{q}}$$

436 with the mass eigenvalues  $m_{\tilde{q}_1}, m_{\tilde{q}_2}$  ( $m_{\tilde{q}_1} < m_{\tilde{q}_2}$ ) and the mixing angle  $\theta_{\tilde{q}}$  ( $-\pi/2 < \theta_{\tilde{q}} \leq \pi/2$ ).

### 437 1.2.3 Phenomenology of Supersymmetry

438 As previously mentioned, the introduction of SUSY particles overcomes the problem of  
439 an unnatural fine-tuning to the Higgs mass due to its quadratic corrections, given that  
440 the stops have masses typically around 1 TeV.

**441 *R-parity***

**442** The most general MSSM can contain operators that violate baryon and/or lepton number,  
**443** thus allowing proton decays. The non-observation of proton decays forbids the existence  
**444** of such terms. A possibility to avoid these operators is to introduce a new discrete sym-  
**445** metry named *R-parity*. The conserved quantum number is defined as;

$$P_R = (-1)^{3(B-L)+2s} \quad (1.21)$$

**446** where  $B$ ,  $L$ , and  $s$  are the baryon, lepton, and spin number, respectively.

**447** If a certain SUSY model is *R*-parity conserving, then the SM particles have  $R = 1$  and  
**448** SUSY partners have  $R = -1$ . When *R*-parity conservation is imposed on MSSM models,  
**449** the mixing between particles and sparticles cannot occur, resulting in the number of SUSY  
**450** particles to be even at every interaction vertex. Furthermore, all sparticles must be pair-  
**451** produced and the Lightest Supersymmetric Particle (LSP) has to be stable and can be a  
**452** good Dark Matter candidate.

**453** Although the SUSY searches in a *R*-parity violating (RPV) scenario have been ex-  
**454** tensively investigated by the particle-physics community, in this work only *R*-parity con-  
**455** serving (RPC) models, where the  $\tilde{\chi}_1^0$  is assumed to be the LSP, were considered.

**456 **Phenomenological MSSM (pMSSM)****

**457** As mentioned in 1.2.2, once the SUSY soft breaking occurred, the unconstrained MSSM  
**458** has more than 100 parameters in addition to the Standard Model ones. However, this  
**459** makes the SUSY searches, e.g. finding regions, in parameter space, that are consistent  
**460** with the data, rather impractical. Under the following three assumptions;

**461** • no new source of CP-violation (CKM matrix is the only source)

**462** • no Flavour Changing Neutral Currents

**463** • first- and second-generation universality

**464** the number of free parameters can be reduced down to 19. The introduction of such para-  
**465** meters, summarised in Table 1.3, defines the so-called phenomenological MSSM (pMSSM).  
**466** Such parameter space is still rather large and it makes pMSSM searches extremely chal-  
**467** lenging and difficult to exclude. To overcome this problem *simplified models* are introduced.  
**468** In other words, a certain signal process is extracted from the model and only particles  
**469** contributing to a certain decay mode will be considered, e.g.  $\tilde{t}_1 \rightarrow t + \tilde{\chi}_1^0$  only targets the

Table 1.3: Parameters in the pMSSM.

Parameter	Description	N. of parameters
$M_1, M_2, M_3$	Bino, Wino and gluino masses	3
$M_A$	pseudoscalar Higgs boson mass	1
$\mu$	higgsino mass	1
$m_{\tilde{q}}, m_{\tilde{u}_R}, m_{\tilde{d}_R}$ , $m_{\tilde{Q}_L}, m_{\tilde{t}}, m_{\tilde{b}}$	first- and second-generation squark masses third generation squark masses	3 3
$m_{\tilde{l}}, m_{\tilde{e}_R}$ $m_{\tilde{L}}, m_{\tilde{\tau}_R}$	first- and second-generation slepton masses third-generation slepton masses	2 2
$A_t, A_b, A_\tau$	third-generation trilinear couplings	3
$\tan \beta$	two-higgs-doublet fields VEVs ratio	1

470 2-body decay ignoring the remaining SUSY mass spectrum. The number of parameters  
471 will then boil down to 2;  $m_{\tilde{t}}$  and  $m_{\tilde{\chi}^0}$ , allowing the reinterpretation of the results and  
472 providing a powerful tool to constrain various models.

473 In this work only analyses laying their theoretical assumptions on such simplified  
474 models will be presented.

#### 475 Phenomenology of the top squark

476 Fig. 1.5 shows SUSY particles production cross-sections for squarks that do not contrib-  
477 ute to gluino production diagrams and vice versa, i. e. treating squarks and gluinos as  
478 *decoupled* making the cross-section of squark pair-production be the same for all famil-  
479 ies. While gluinos production cross-sections are fairly large, SUSY electroweak produc-  
480 tion cross-sections of neutralinos and charginos are considerably lower. Sleptons pro-  
481 duction cross-section, which is not displayed, would sit just below higgsino-like char-  
482 gino/neutralino production cross-section.

483 Due to the cross-section being around a factor of six smaller than  $t\bar{t}$  production (when  
484  $m_{\tilde{t}_1} \sim m_t$ ), third-generation SUSY analyses are very challenging. Furthermore, the cross-  
485 section of such processes dramatically decreases with increasing  $m_{\tilde{q}}$ . Nonetheless, for  
486 example, searches for direct  $\tilde{t}_1$  production with  $\tilde{t}_1 \rightarrow t + \tilde{\chi}_1^0$  are sensitive in a scenario  
487 where  $m_{\tilde{t}_1} \gg m_t + m_{\tilde{\chi}_1^0}$  as the large  $E_T^{\text{miss}}$ , from the neutralinos, provides discriminating  
488 power for  $t\bar{t}$  rejection.

489 There exists various decay modes of pair-produced stops, depending on the masses  
490 of the decay products;

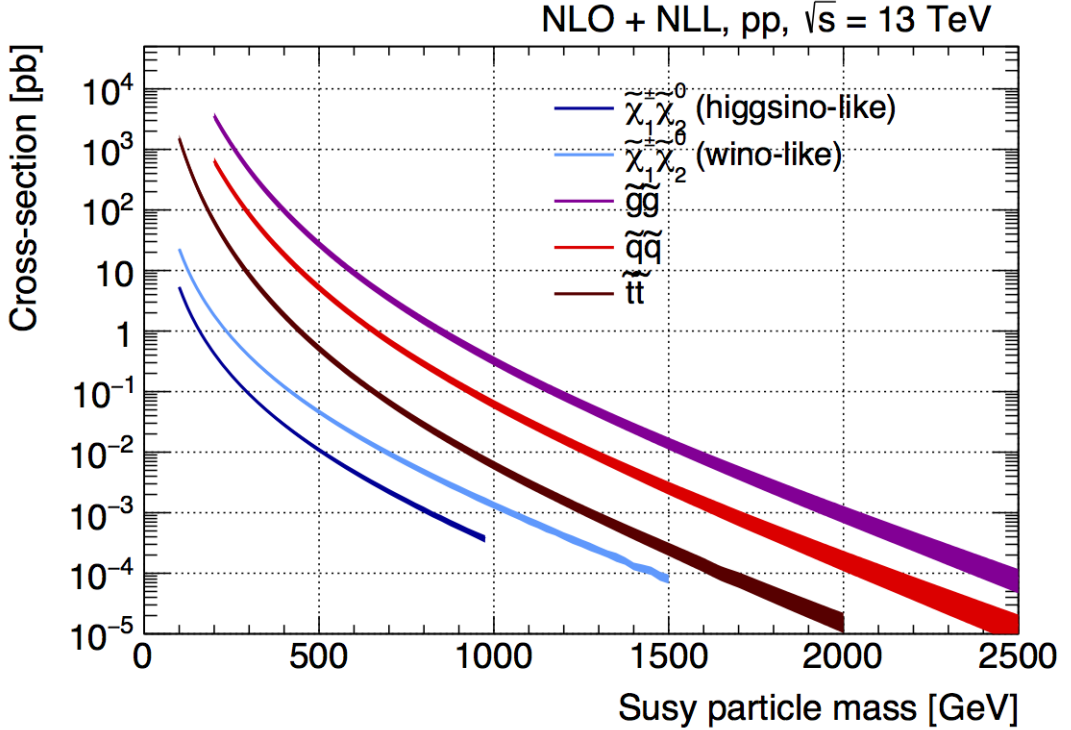


Figure 1.5: NLO+NLL production cross-sections as a function of mass at  $\sqrt{s} = 13$  TeV [2]

- 491     •  $\tilde{t} \rightarrow t \tilde{\chi}^0$
- 492     •  $\tilde{t} \rightarrow b \tilde{\chi}^\pm \rightarrow b W \tilde{\chi}^0$  (on/off-shell  $W$ ) or  $\tilde{t} \rightarrow b W \tilde{\chi}^0$  (off-shell top)
- 493     •  $\tilde{t} \rightarrow c \tilde{\chi}^0$
- 494     •  $\tilde{t} \rightarrow b f f' \tilde{\chi}^0$

495     Figure 1.6 shows a schematic representation of the parameter space  $(m_{\tilde{t}_1}, m_{\tilde{\chi}_1^0})$  and the  
496     different region where each of the above-mentioned process dominates.

497     In the models considered in this work, either  $\tilde{\chi}_2^0$  or  $\tilde{\chi}_1^\pm$  is assumed to be the so-called  
498     next lightest supersymmetric particle (NLSP). Three different decay scenarios were con-  
499     sidered in this work; (a) where both top squarks decay via  $\tilde{t} \rightarrow t^{(*)} \tilde{\chi}_1^0$ <sup>1</sup>; (b) at least one  
500     of the stops decays via  $\tilde{t} \rightarrow b \tilde{\chi}_1^\pm \rightarrow b W^{(*)} \tilde{\chi}_1^0$ ; (c) where  $m_{\tilde{\chi}_2^0}$  is small enough to allow  
501     one stop to decay via  $\tilde{t} \rightarrow t \tilde{\chi}_2^0 \rightarrow h/Z \tilde{\chi}_1^0$ . Here,  $h$  is the SM Higgs boson (125 GeV),  
502     as illustrated in Figure 1.7(a)–(c), respectively. Furthermore, top squarks can also be in-  
503     directly produced through the so-called gluino-mediated stop production, as shown in  
504     Figure 1.7(d).

<sup>1</sup> The symbol (\*) indicates that the decay can occur with the top quark being produced off-shell (region between the second and third dashed line in Fig. 1.6)

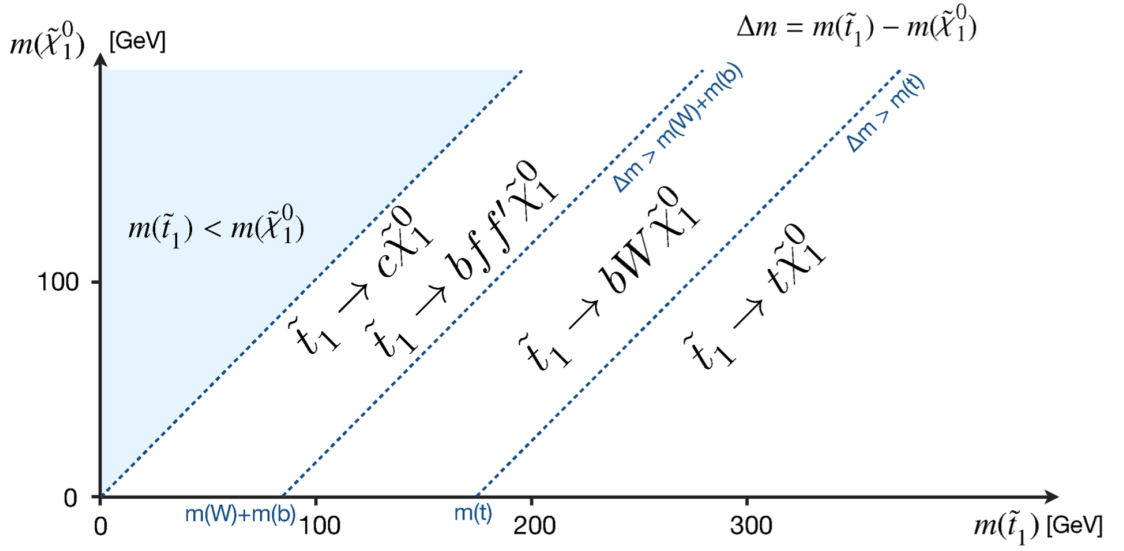


Figure 1.6: Illustration of stop decay modes in the  $(m_{\tilde{t}_1}, m_{\tilde{\chi}_1^0})$  mass place where the  $\tilde{\chi}_1^0$  is assumed to be the lightest supersymmetric particle. The dashed blue lines indicate thresholds separating regions where different processes dominate.

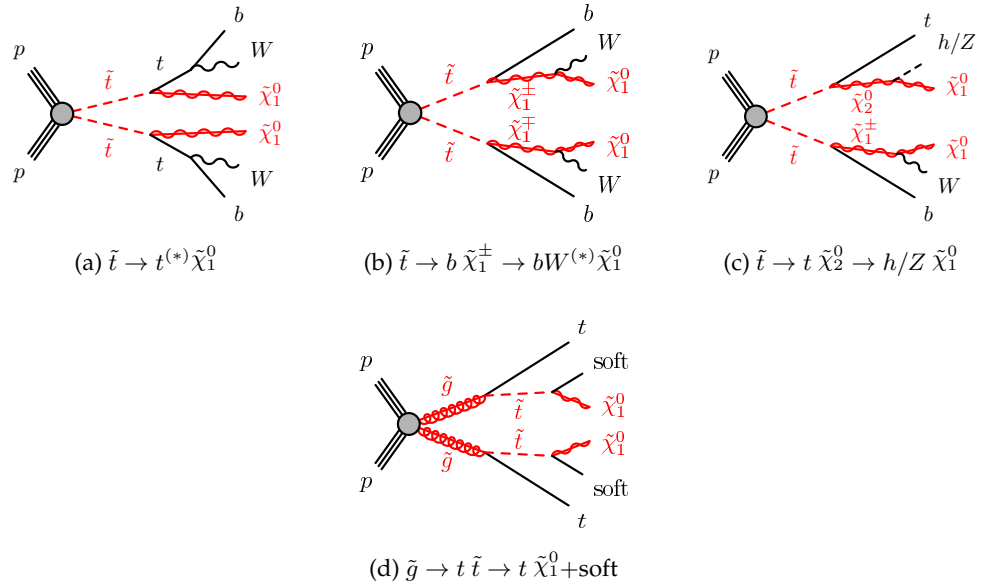


Figure 1.7: Diagrams of the decay topologies of the signal models considered in this work. The term “soft” refers to decay products that have transverse momenta below the detector thresholds.

505    **2** | **The ATLAS Experiment at the**  
 506    **LHC**

507

*We are rather like children, who  
 must take a watch to pieces to see  
 how it works*

---

Sir Ernest Rutherford

508    ATLAS (A Toroidal LHC ApparatuS) is one of the four main experiments (ATLAS,  
 509    CMS, ALICE, LHCb) taking data at a center-of-mass energy of 13 TeV using beams de-  
 510    livered by the Large Hadron Collider (LHC). In this chapter an overview of the LHC will  
 511    be given in Section 2.1, then the ATLAS detector will be described in Section 2.2, and fi-  
 512    nally the Trigger system, used to cleverly store the data, will be described in Section 2.3. A  
 513    more in-depth description of the Trigger algorithms I have been involved in will be given  
 514    in Chapter 3.

515    **2.1 The LHC**

516    As of today, the LHC is the world's largest and most powerful particle accelerator. It was  
 517    designed to help answer some of the fundamental open questions in particle physics by  
 518    colliding protons at an unprecedented energy and luminosity. It is located at the European  
 519    Organisation for Nuclear Research (CERN), in the Geneva area, at a depth ranging from  
 520    50 to 175 metres underground. It consists of a 27-kilometre ring made of superconducting  
 521    magnets, and inside it two high-energy particle beams travel in opposite directions and  
 522    in separate beam pipes.

523    The beams are guided around the ring by a strong magnetic field generated by coils -  
 524    made of special electric cables - that can operate in a superconducting regime. 1232 super-  
 525    conducting dipole and 392 quadrupole magnets, with an average magnetic field of 8.3 T,

526 are employed and kept at a temperature below 1.7 K, in order to preserve their supercon-  
 527 ducting properties. The formers are used to bend the beams and the latters to keep them  
 528 focused while they get accelerated.

529 The collider first went live on September 2008 even though, due to a magnet quench  
 530 incident that damaged over 50 superconducting magnets, it has been operational since  
 531 November 2009 when low-energy beams circulated in the tunnel for the first time since the  
 532 incident. This also marked the start of the main research programme and the beginning  
 533 of the so-called Run 1: first operational run (2009 - 2013).

### 534 Performance of the LHC

535 In June 2015 the LHC restarted delivering physics data, after a two-year break, the so-  
 536 called Long Shutdown 1 (LS1), during which the magnets were upgraded to handle the  
 537 current required to circulate 7-TeV beams. It was the beginning of the so-called Run 2 -  
 538 second operational run (2015-2018) - during which LHC has collided up to  $10^{11}$  bunches  
 539 of protons every 25 ns at the design luminosity - the highest luminosity the detector was  
 540 designed to cope with - of  $2 \cdot 10^{34} \text{ cm}^{-2} \text{s}^{-1}$ . The definition of the luminosity is:

$$\mathcal{L} = f \frac{n_b N_1 N_2}{4\pi\sigma_x\sigma_y} \quad (2.1)$$

541 where  $N_1$  and  $N_2$  are the number of protons per bunch in each of the colliding beams,  $f$   
 542 is the revolution frequency of the bunch collisions,  $n_b$  the number of proton per bunch,  
 543 and  $\sigma_x$  and  $\sigma_y$  are the horizontal and vertical dimensions of the beam. The luminosity is  
 544 strictly related to the number of collisions occurring during a certain experiment via the  
 545 following:

$$\mathcal{N}_{\text{event}} = \mathcal{L}\sigma_{\text{event}} \quad (2.2)$$

546 where  $\sigma_{\text{event}}$  is the cross section of the process under investigation. It has not only collided  
 547 protons but also heavy ions, in particular lead nuclei at  $\sqrt{s_{NN}} = 5.02 \text{ TeV}$ , at a luminosity  
 548 of  $10^{27} \text{ cm}^{-2} \text{s}^{-1}$  [23].

### 549 Acceleration stages

550 Before reaching the maximum energy, the proton beams are accelerated by smaller ac-  
 551 celerators through various stages. Figure 2.1 shows a sketch of the CERN's accelerator  
 552 complex. It all begins at the linear accelerator LINAC 2. Here protons are accelerated up  
 553 to 50 MeV, and then injected in the Proton Synchrotron Booster (PSB) where they reach

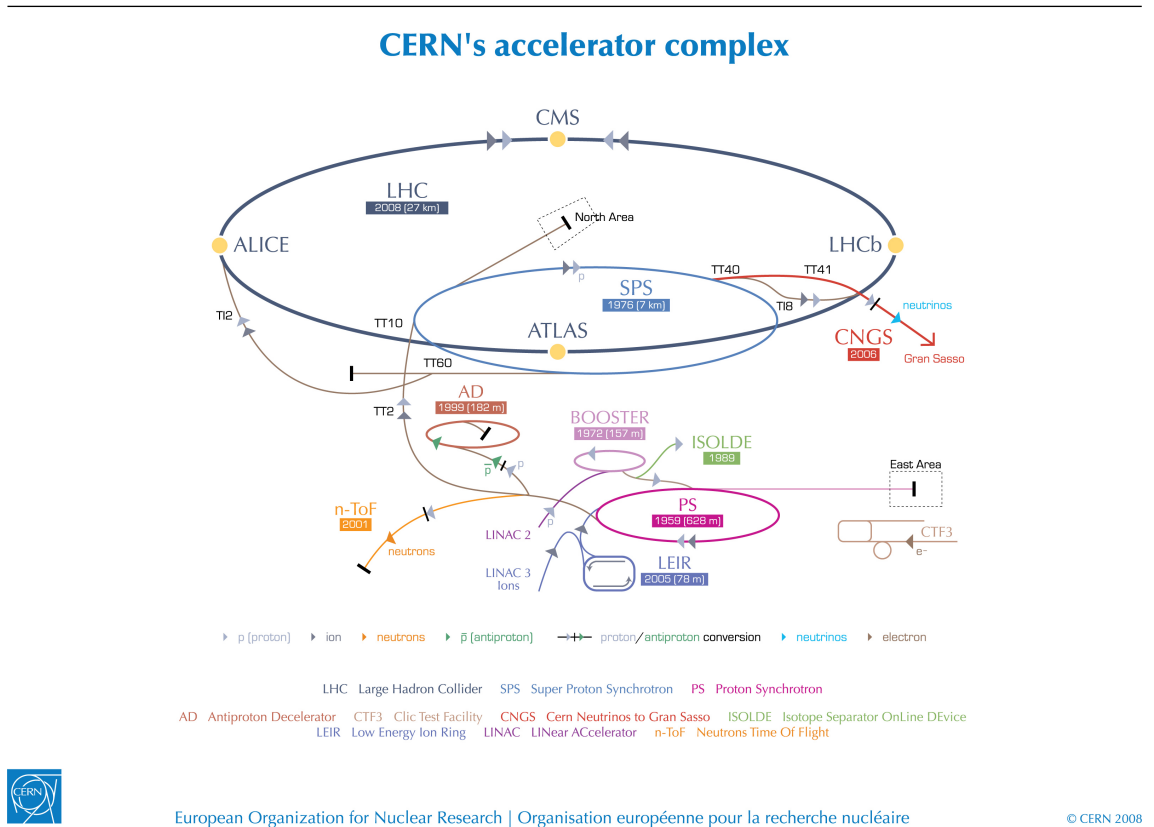


Figure 2.1: CERN Accelerator complex. The LHC is the last ring (dark grey line). Smaller machines are used for early-stage acceleration and also to provide beams for other experiments [3].

554 1.4 GeV. The next stage is the Proton Synchrotron (PS), which boosts the beams up to 25  
 555 GeV and then the Super Proton Synchrotron (SPS) makes them reach energies up to 450  
 556 GeV. Eventually, the beams are injected in bunches with a 25 ns spacing into the LHC,  
 557 where they travel in opposite directions, while they are accelerated to up to 13 TeV. Once  
 558 the bunches reach the maximum energy, they are made collide at four different points,  
 559 inside four experiments around the ring [24].

560 The heavy ion beams acceleration procedure is slightly different. Their journey starts  
 561 at LINAC 3 first, and the Low Energy Ion Ring (LEIR) then, before they make their way  
 562 into the PS where they follow the same path as the protons [24].

563 The four large detectors on the collision points are; the multi-purpose detectors A Tor-  
 564 oidal LHC ApparatuS (ATLAS), and Compact Muon Solenoid (CMS) [25], Large Hadron  
 565 Collider beauty (LHCb) [26], which focuses on flavour physics, and A Large Ion Collider  
 566 Experiment (ALICE) [27] which specialises in heavy ion physics. The *big four* are not the  
 567 only experiments at the CERN's accelerator complex. There also are smaller experiments  
 568 based at the the four caverns about the collision points e.g. TOTEM, LHCf and MoEDAL,  
 569 but this will not be discussed any further in this thesis.

## 570 2.2 The ATLAS Detector

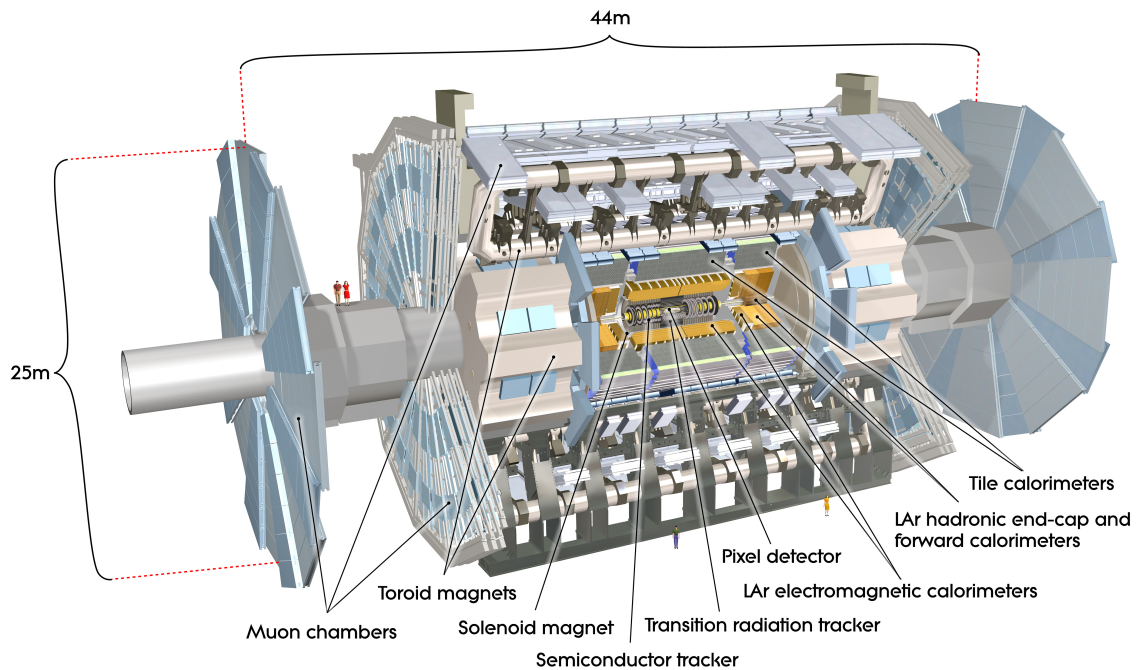


Figure 2.2: Cut-away view of the ATLAS detector. The dimensions of the detector are 25 m in height and 44 m in length. The overall weight of the detector is approximately 7000 tonnes [3].

571       ATLAS is a general-purpose detector designed to collect data with the highest luminosity provided by the LHC. It is located at CERN’s Point 1 cavern and it measures about  
 572       45 m in length and 25 m in diameter. It has a forward-backward symmetric cylindrical  
 573       geometry with respect to the interaction point and it is designed to reconstruct and mea-  
 574       sure physics objects such as electrons, muons, photons and hadronic jets. Its design was  
 575       optimised to be as sensitive as possible to the discovery of the Higgs boson and beyond-  
 576       the-Standard-Model (BSM) physics. In fact, thanks to the other sub-systems, ATLAS is  
 577       able to observe all possible decay products by covering nearly  $4\pi$  steradians of solid angle.  
 578

579       In Figure 2.2 a cut-away view of ATLAS with all its components is shown. The inner-  
 580       most layer is the Inner Detector (ID) which is the core of the tracking system and consists  
 581       of a Pixel, a Silicon micro-strip tracker (SCT), and a Transition Radiation Tracker (TRT).  
 582       It is submerged in a 2 T magnetic field, generated by a thin superconducting solenoid,  
 583       which bends all the charged particles’ trajectories allowing transverse momentum meas-  
 584       urement. The electromagnetic and hadronic calorimeters form the next layer and they are  
 585       both used to perform precise energy measurements of photons, electrons, and hadronic  
 586       jets. Finally, the outermost layer corresponds to the Muon Spectrometer (MS) which, to-

587 gether with the ID, enclosed in a toroidal magnetic field, allows precise measurement of  
 588 momentum and position of muons. These sub-detectors will be discussed in more detail  
 589 in the following sections.

## 590 The ATLAS coordinate system

591 A coordinate system is taken on for the spatial definition of the sub-systems and kinematic  
 592 measurement of physics processes. Such system is defined starting from the interaction  
 593 point, defined as the origin. The  $z$ -axis is defined by the beam direction and the  $x - y$   
 594 plan, as transverse to the beam direction.

595 A quantity, known as pseudorapidity, ( $\eta$ ), is defined to describe the angle of a particle  
 596 coming out of the collision, with respect to the beam axis:

$$\eta \equiv -\ln(\tan(\theta/2))$$

597 Here  $\theta$  is the polar angle. The azimuthal angle,  $\phi$ , is defined around the beam axis and  
 598 the polar angle. In the  $(\eta, \phi)$  space a distance  $\Delta R$  can be therefore defined as

$$\Delta R = \sqrt{\Delta\eta^2 + \Delta\phi^2}$$

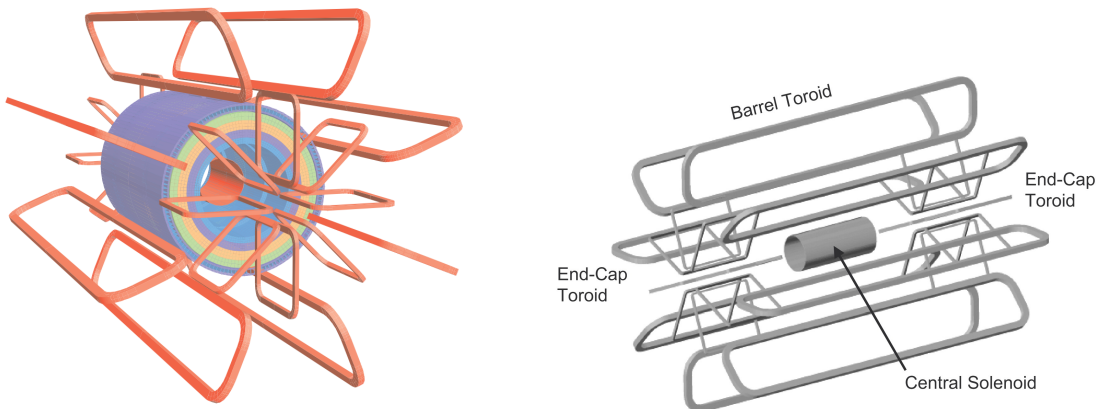
599 where  $\Delta\eta$  and  $\Delta\phi$  are the differences in pseudorapidity and azimuthal angle between any  
 600 two considered objects. A central and a forward region of pseudorapidity are also defined  
 601 such that the detector components are described as part of the *barrel* if they belong to the  
 602 former or as part of the *end-caps* if they belong to the latter.

### 603 2.2.1 The Magnet System

604 The ATLAS magnet system, 26 m long with a 22 m diameter, generates the magnetic field  
 605 needed to bend the trajectories of charged particles in order to perform momentum meas-  
 606 urement. Figure 2.3a and 2.3b show the geometry of the system and its components,  
 607 which are made of NbTi - superconducting material - and will be described in the follow-  
 608 ing paragraphs.

### 609 The Central Solenoid

610 With an axial length of 5.8 m, an inner radius of 2.46 m, and an outer radius of 2.56 m, the  
 611 central solenoid magnet is located between the ID and the ECAL. Its function is to bend  
 612 the charged particles that go through the ID and it is aligned on the beam axis providing a  
 613 2 T axial magnetic field that allows accurate momentum measurement up to 100 GeV [28].



(a) Geometry of magnet windings and tile calorimeter steel. The eight barrel toroid coils, with the end-cap coils interleaved are visible. The solenoid winding lies inside the calorimeter volume [4].

(b) Schematic view of the superconducting magnets [28].

Figure 2.3: The ATLAS magnet system.

## 614    The Barrel and the End-cap Toroids

615    Figure 2.3b displays the toroid magnetic system that surrounds the calorimeters. With its  
 616    cylindrical shape this component consists of a barrel and two end-caps toroids, each with  
 617    eight superconducting coils. The system allows accurate measurement of muon momenta  
 618    using a magnetic field of approximately 0.5 T (barrel) for the central regions and 1 T (end-  
 619    cap) for the end-cap regions, respectively, which bends the particles in the  $\theta$  direction.

### 620    2.2.2    The Inner Detector

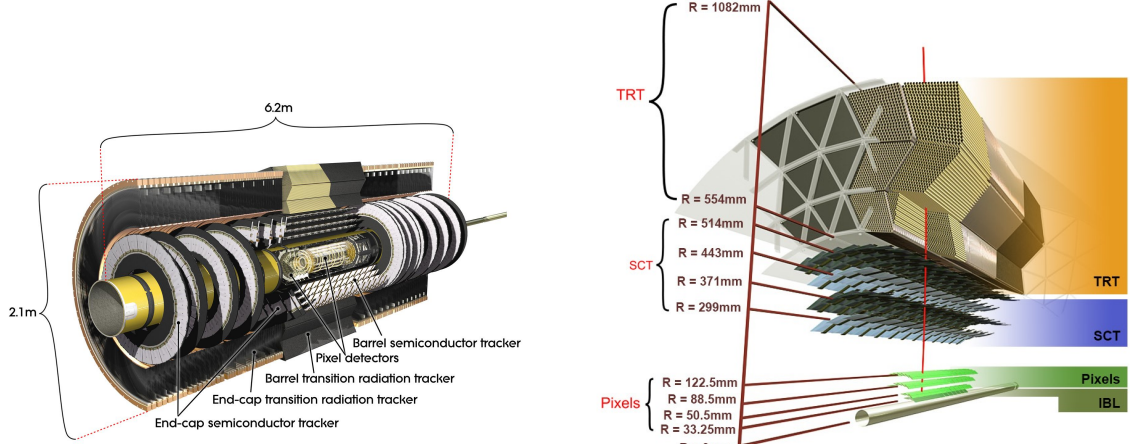
621    The Inner Detector (ID) [29] is the innermost component of the ATLAS detector i. e. the  
 622    nearest sub-detector to the interaction region and it is used to reconstruct charged particle  
 623    tracks used in the selection of physics objects. In fact, it allows robust track reconstruction,  
 624    with accurate impact parameter resolution ( $\sim 20\mu m$ ) and precise primary and secondary  
 625    vertex reconstruction for charged particles (tracks) above 500 MeV and within  $|\eta| < 2.5$ .

626       The ID is comprised of independent and concentric sub-systems, which are all shown  
 627    in Figure 2.4:

628       • Insertable B-Layer (IBL):

629           innermost Pixel Detector layer added during ATLAS Run 2 upgrade (2013/2014) to  
 630           improve vertexing and impact parameter reconstruction;

631       • Silicon Pixel Tracker (Pixel):



(a) Overview of the ATLAS ID with labels and dimensions.

(b) Diagram of the ATLAS ID and its sub-detectors.

Figure 2.4: The ATLAS Inner Detector

made of silicon pixel layers and used mainly for reconstructing both the primary and secondary vertices in an event;

• SemiConductor Tracker (SCT):

comprised of silicon microstrip layers; thanks to its resolution ( $17 \times 580 \mu\text{m}$ ) it can accurately measure particle momenta;

• Transition Radiation Tracker (TRT):

final layer comprised of various layers of gaseous straw tube elements surrounded by transition radiation material.

These sub-detectors will be discussed in the following sections.

### IBL

The IBL [30] is the innermost Pixel Detector layer as shown in Figure 2.4b. It is comprised of 6M channels and each pixel measures  $50 \times 250 \mu\text{m}$ . Its resolution is  $8 \times 40 \mu\text{m}$ . The addition of this new layer brought a considerable improvement on the performance of the Pixel Detector by enhancing the quality of impact parameter reconstruction of tracks. In particular, this was achieved by improving the vertex finding efficiency and the tagging of bottom-quark-initiated jets ( $b$ -jets) which, in case of a B-layer failure, can be restored by the IBL. Besides these improvements, the IBL insertion allowed ATLAS to better cope with high luminosity effects such as the increase in event pile-up, which leads to high occupancy and read-out inefficiency.

## 651 Pixel

652 The Pixel detector is comprised of 1750 identical sensorchip-hybrid modules, each cover-  
 653 ing an active area of  $16.4 \times 60.8$  mm. The total number of modules correspond to roughly  
 654 80 million semiconductor silicon pixels. The nominal pixel size is  $50 \mu\text{m}$  in the  $\phi$  direction  
 655 and  $400 \mu\text{m}$  in the barrel region, along the  $z$ -axis (beam axis) [31]. The reason why such a  
 656 large amount of pixels is employed is justified by the need to cope with the high luminos-  
 657 ity in ATLAS. The silicon pixel detector measures 48.4 cm in diameter and 6.2 m in length  
 658 providing a pseudorapidity coverage of  $|\eta| < 2.5$ . Figure 2.4b shows the three concentric  
 659 barrel layers placed at 50.5 mm, 88.5 mm and 122.5 mm respectively. Furthermore, the  
 660 Pixel detector is made of six disk layers, three for each forward region, such that when a  
 661 charged particle crosses the layers it will generate a signal at least in three space points.  
 662 The fine granularity of such detector allows accurate measurement and precise vertex re-  
 663 construction, as it provides a more accurate position measurement as a large detection  
 664 area is available. In particular, it has a resolution of  $10 \times 115 \mu\text{m}$ .

## 665 SCT

666 The SCT is made of 4088 modules of silicon micro-strip detectors arranged in four con-  
 667 centric barrel layers. It is mainly used for precise momentum reconstruction over a range  
 668  $|\eta| < 2.5$  and it was designed for precision measurement of the position using four points  
 669 (corresponding to eight silicon layers), obtained as track hits when crossing the layers.  
 670 Figure 2.4b shows the structure of the SCT with its four concentric barrel layers with radii  
 671 ranging from 299 mm to 514 mm and two end-cap layers. Each module has an intrinsic  
 672 resolution of  $17 \mu\text{m}$  in the  $R - \phi$  direction and  $580 \mu\text{m}$  in the  $z$  direction. As the SCT is fur-  
 673 ther away from the beam-pipe than the Pixel detector, it has to cope with reduced particle  
 674 density. This allows for reduced granularity maintaining the same level of performance of  
 675 the Pixel detector: SCT can use  $\sim 6.3$  million read-out channels.

## 676 TRT

677 The last and outermost of the sub-systems in the ID is the TRT. It is a gaseous detector  
 678 which consists of 4 mm diameter straw tubes wound from a multilayer film reinforced  
 679 with carbon fibers and containing a  $30 \mu\text{m}$  gold plated tungsten wire in the center. The  
 680 straw is filled with a gas mixture of 70% Xe, 27% CO<sub>2</sub> and 3% O<sub>2</sub> [32]. As shown in  
 681 Figure 2.4b, its section consists of three concentric layers with radii ranging from 544 mm  
 682 to 1082 mm, each of which has 32 modules containing approximately 50,000 straws, 1.44 m

in length, aligned parallel to the beam direction with independent read-out at both ends.  
Both end-cap sections are divided into 14 wheels, with roughly 320,000 straws in the R-direction. The average 36 hits per track in the central region of the TRT allow continuous tracking to enhance pattern recognition and momentum resolution in the  $|\eta| < 2.5$  region.  
It also improves the  $p_T$  resolution for longer tracks.

### 2.2.3 The Calorimeters

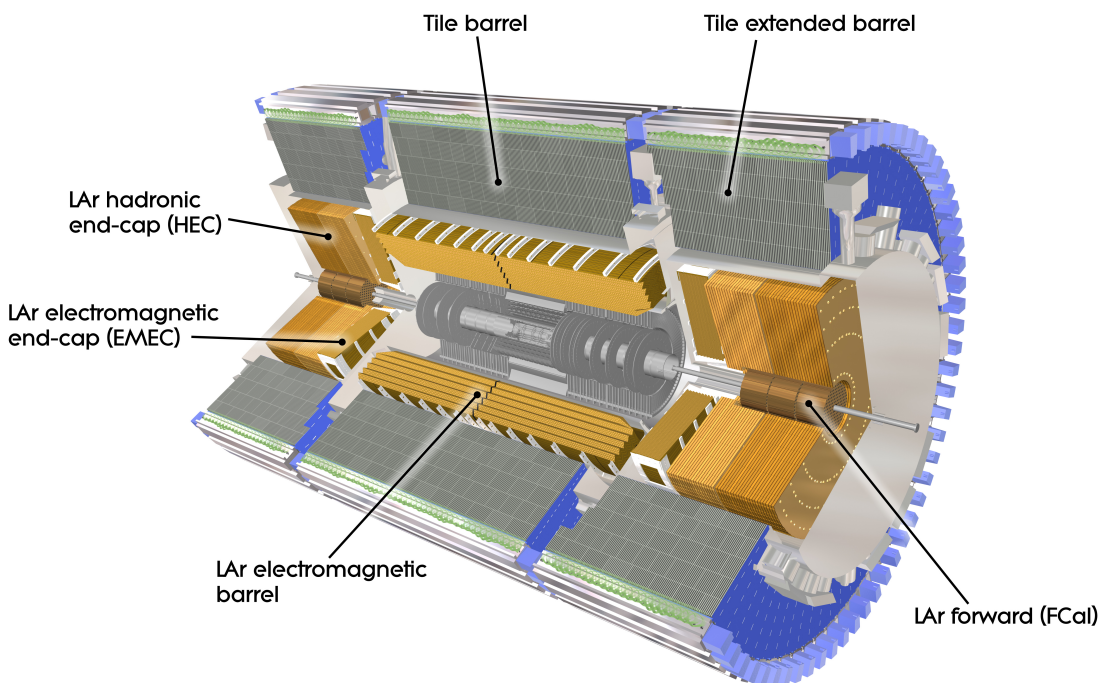


Figure 2.5: A computer generated image of the full calorimeter.

The ATLAS Calorimeter system, shown in Figure 2.5, is comprised of two main subsystems; the electromagnetic calorimeter (ECAL) and hadronic calorimeter (HCAL), which are designed to stop and measure the energy of electromagnetic-interacting and hadronic particles respectively. The combination of the two provides full coverage in  $\phi$  and  $|\eta| < 4.95$ . Particles slow down and lose energy generating showers when crossing different layers. The ECAL is comprised of one barrel and two end-cap sectors employing liquid Argon (LAr). The showers hereby develop as electrons pairs which are then collected. The HCAL is also comprised of one barrel and two end-cap sectors. The sensors in the barrel of the HCAL are tiles of scintillating plastic whereas LAr is employed for the end-cap. A forward region, the closest possible to the beam, is covered by a LAr forward calorimeter (FCal). The LAr and Tile Calorimeter will be briefly discussed in the

700 following paragraphs.

### 701 The Liquid Argon Calorimeters

702 The ECAL is comprised of multiple layers of liquid Argon (LAr) sampler and lead ab-  
703 sorber. The choice of its accordion-geometry design brought two main advantages; full  
704  $\phi$  coverage with no non-interactive regions (no cracks); fast extraction of signals coming  
705 from both front or rear end of the electrodes. It is made of two half-barrel wheels, both  
706 placed in the barrel cryostat, that provide a pseudorapidity coverage up to  $|\eta| < 1.475$   
707 and two end-cap detectors providing  $1.375 \leq |\eta| \leq 3.20$  coverage in two end-cap cryo-  
708 stats. The junction between the barrel and end cap components defines the crack region  
709 and any signal coming from the crack region is therefore discarded.

710 In the  $|\eta| < 1.8$  region there is an additional layer, placed at the front of the calorimeter,  
711 that is made of a thin (0.5 cm in the end-cap and 1.1 cm in the barrel) LAr layer with  
712 no absorber [33]. This additional layer was designed to correct for the energy lost, as  
713 particles enter the calorimeter, by taking a measurement just before the majority of the  
714 electromagnetic shower is developed.

### 715 The Tile calorimeter

716 The main purpose of the hadronic calorimeter is to measure the energy of hadronic showers.  
717 It is built employing steel and scintillating tiles coupled to optical fibres which are read  
718 out by photo-multipliers. As shown in Figure 2.5, the HCAL is made up of three cylin-  
719 ders; a central barrel, 5.64 m long covering a region  $|\eta| < 1.0$ , and two extended barrel,  
720 2.91 m long covering a reigon  $0.8 < |\eta| < 1.7$ . Each cylinder is made up of 64 modules  
721 and each module is in turn made up of three layers. Ultimately, the smallest section of the  
722 calorimeter module is a cell with a  $\Delta\phi \times \Delta\eta = 0.1 \times 0.1$  granularity for the two innermost  
723 layers and  $\Delta\phi \times \Delta\eta = 0.2 \times 0.1$  for the outermost one.

#### 724 2.2.4 The Muon Spectrometer

725 The MS [34], shown in Figure 2.6, is the outermost sub-system of the whole ATLAS de-  
726 tector. As such, it surrounds the calorimeters and its main function is to perform precision  
727 measurement of muons momenta. The deflection of muon tracks employing large super-  
728 conducting air-core toroid magnets and high-precision tracking chambers is at the heart  
729 of such high precision measurement.

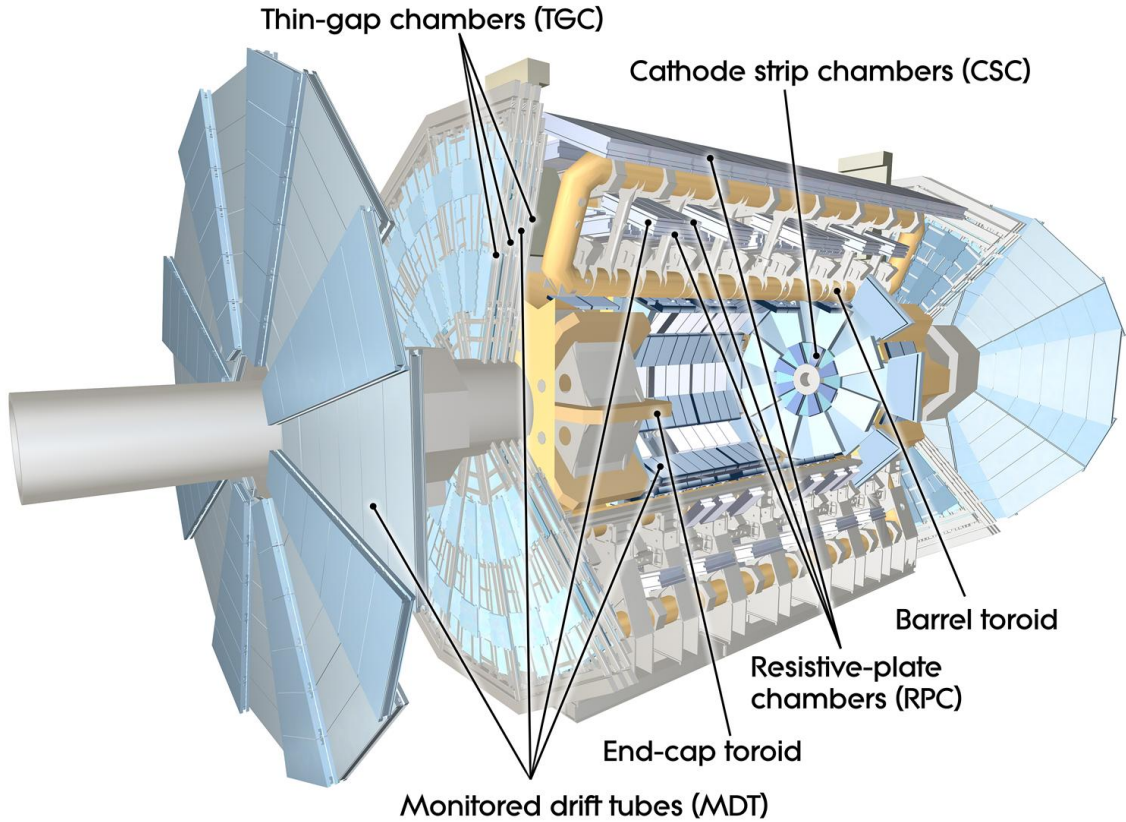


Figure 2.6: Cut-away view of the ATLAS muon system [4].

730        The MS is comprised of one large barrel toroid, covering the region  $|\eta| \leq 1.4$ , and  
 731        two end-cap toroids, covering  $1.6 < |\eta| \leq 2.7$  which are employed together to achieve the  
 732        track-bending effect wanted. The magnitude of the magnetic field in the barrel, generated  
 733        by eight large superconducting coils, ranges from 0.5 to 2 T.

734        Around the beam axis, three cylindrical layers make way for the chambers, placed in  
 735        planes perpendicular to the beam, used to measure tracks.

736        Monitored Drift Chambers (MDTs) are employed over most of the pseudorapidity  
 737        range to provide precision measurement of track coordinates in the bending direction.  
 738        Cathode Strip Chambers (CSCs) are instead employed at large pseudorapidity ( $2 < |\eta| <$   
 739        2.7). Finally, in the end-cap regions Thin-Gap Chambers (TGCs) together with Resistive-  
 740        Plate Chambers (RPCs) are dedicated to the Trigger System discussed in Section 2.3.

## 741        2.3 The ATLAS Trigger System

742        The ATLAS Trigger System is at the heart of data taking. It is an essential component of  
 743        any nuclear or particle physics experiment since it is responsible for deciding whether or  
 744        not to store an event for later study [5]. The ATLAS Trigger system is employed to reduce

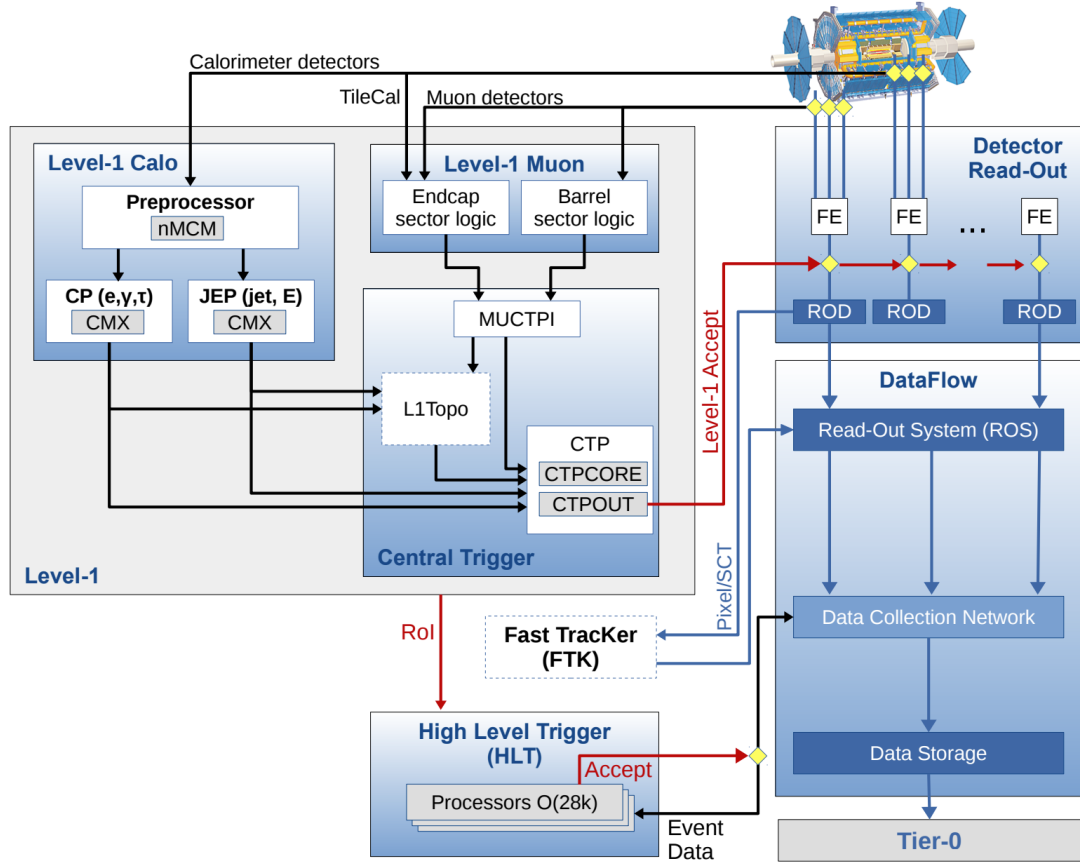


Figure 2.7: The ATLAS TDAQ system. L1Topo and FTK were being commissioned during 2015 and not used for the results shown in this thesis [5].

745 the event rate from  $\sim 40 \text{ MHz}$ <sup>1</sup> bunch-crossing<sup>2</sup> to  $\sim 200 \text{ Hz}$  which corresponds to roughly  
 746 300 MB/s.

747 The Trigger and Data Acquisition (TDAQ) system shown in Figure 2.7 consists of a  
 748 hardware-based first level trigger (L1) and a software-based high-level trigger (HLT). The  
 749 L1 trigger decision is formed by the Central Trigger Processor (CTP), which receives in-  
 750 puts from the L1 calorimeter (L1Calo) and L1 muon (L1Muon) triggers. The first level  
 751 (L1), which was designed to perform the first selection step, is a hardware-based system  
 752 that uses information from the calorimeter and muon subdetectors. It also defines the  
 753 so-called Regions of Interest (RoIs) within the detector to be investigated by the next level  
 754 trigger, the HLT. Additionally, a Fast TracKer (FTK) system [35] (not yet installed) will  
 755 provide global ID track reconstruction at the L1 trigger rate using lookup tables stored in

<sup>1</sup> The LHC delivers beams with a bunch-spacing of 25 ns.

<sup>2</sup> The term bunch-crossing is hereby used when referring to a collision between two bunches of protons. Since only a certain fraction of the total momentum carried by each proton contributes to the collision, an average number of interactions per bunch-crossing,  $\langle \mu \rangle$  is used.

756 custom associative memory chips for the pattern recognition. The FPGA-based track fitter  
757 will perform a fast linear fit and the tracks are made available to the HLT. This system will  
758 allow the use of tracks at much higher event rates in the HLT than is currently affordable  
759 using CPU systems. However, the upgrade of the ATLAS trigger will not be discussed  
760 any further.

761 In the next sections the L1 and HLT will be briefly described.

### 762 2.3.1 Level 1 Trigger

763 The Level 1 Trigger identifies Regions of Interest (RoIs)<sup>3</sup> and passes these to HLT which  
764 will perform further investigations. Furthermore, in order to decide whether or not the  
765 event processing will continue, L1 selection uses only information coming from some  
766 parts of the detector to keep the input rate to a maximum of 100 kHz. L1 is implemented  
767 in fast custom electronics to keep the latency<sup>4</sup> below 2.5  $\mu$ s. Event data from other sub-  
768 syststem are temporarily stored in memories whilst L1 decision is taken.

769 The L1 topological trigger (L1-Topo) [36] is feeded with energy and direction inform-  
770 ation, about the objects found by the L1 calorimeter and the muon trigger, which will be  
771 processed by dedicated algorithms implemented in its own FPGAs. However, due to the  
772 100 kHz read-out rate, not all the information collected by L1-Topo will be sent to the HLT,  
773 but only part of it. In order to properly seed the ROI-guided HLT reconstruction, specific  
774 objects in combination with the correct topological criteria must be employed.

### 775 2.3.2 High-Level Trigger

776 The HLT is used to reduce the output rate down to 1 kHz and it has a  $\sim$ 200 ms average  
777 decision time. Events that pass L1 trigger are then processed by the HLT using finer-  
778 granularity calorimeter information, precision measurements from the MS and tracking  
779 information from the ID. The HLT reconstruction can be run within RoIs identified at L1  
780 or a so-called full-scan on the full detector can be performed. The track reconstruction in  
781 the Inner Detector is an essential component of the trigger decision in the HLT and it will  
782 be discussed more in detail in Chapter 3

---

<sup>3</sup>  $\eta - \phi$  regions where event features have been found by the L1 selection process.

<sup>4</sup> Time needed by an electric signal to get to the front-end electronics.

783 **3** | The *b*-jet Trigger Signature in AT-  
784 LAS

785 In this chapter the monitor and performance of the bottom-quark-initiated jet (*b*-jet) sig-  
786 nature trigger, this being the author’s “technical/qualification task” to become a qualified  
787 member of the experiment, will be discussed. The efficiencies of some of the Run 2 *b*-jet  
788 triggers were evaluated using  $3.8 \text{ fb}^{-1}$  of  $pp$  collisions data collected in 2015 with 25 ns  
789 bunch-spacing.

790 The qualification task

791 **3.1 Trigger Efficiency**

# 792 **4** | Event Simulation and Reconstruction

793

794 bla bla bla

795 **4.1 Event Generation**

796 bla bla

797 **4.1.1 Parton Distribution Functions (PDFs)**

798 bla bla bla

799 **4.1.2 Matrix Element Calculation**

800 bla bla bla

801 **4.1.3 Parton Showers**

802 bla bla bla

803 **4.1.4 Hadronisation**

804 bla bla bla

805 **4.2 Detector Simulation**

806 bla bla bla

807 **5** | Stop searches in final states with  
808 jets and missing transverse en-  
809 ergy

<sup>810</sup> **6** | Results and Statistical Interpretations

<sup>811</sup>

812 Trigger

813 bla vlas bla

# Bibliography

- [1] ATLAS Collaboration, "Summary plots from the atlas standard model physics group." [https://atlas.web.cern.ch/Atlas/GROUPS/PHYSICS/CombinedSummaryPlots/SM/ATLAS\\_a\\_SMSummary\\_TotalXsect/ATLAS\\_a\\_SMSummary\\_TotalXsect.png](https://atlas.web.cern.ch/Atlas/GROUPS/PHYSICS/CombinedSummaryPlots/SM/ATLAS_a_SMSummary_TotalXsect/ATLAS_a_SMSummary_TotalXsect.png). viii, 9
- [2] C. Borschensky, M. Krämer, A. Kulesza, M. Mangano, S. Padhi, T. Plehn, and X. Portell, *Squark and gluino production cross sections in pp collisions at  $\sqrt{s} = 13, 14, 33$  and 100 TeV*, *Eur. Phys. J.* **C74** no. 12, (2014) 3174, [arXiv:1407.5066 \[hep-ph\]](https://arxiv.org/abs/1407.5066). viii, 18
- [3] C. Lefèvre, *The CERN accelerator complex*, <http://cds.cern.ch/record/1260465>. ix, 22, 23
- [4] ATLAS Collaboration, *The ATLAS experiment at the CERN Large Hadron Collider*, *Journal of Instrumentation* **3** no. 08, (2008) S08003. <http://stacks.iop.org/1748-0221/3/i=08/a=S08003>. ix, 25, 30
- [5] A. Collaboration, *Performance of the ATLAS Trigger System in 2015*, *Eur. Phys. J.* **C77** (2017), [arXiv:1611.09661 \[hep-ex\]](https://arxiv.org/abs/1611.09661). ix, 30, 31
- [6] M. Herrero, *The Standard Model*, <https://arxiv.org/abs/hep-ph/9812242>. 3
- [7] ATLAS Collaboration, *Observation of a New Particle in the Search for the Standard Model Higgs Boson with the ATLAS Detector at the LHC*, *Phys.Lett.* **B716** (2012), [arXiv:1207.7214 \[hep-ex\]](https://arxiv.org/abs/1207.7214). 3
- [8] CMS Collaboration, *Observation of a new boson at a mass of 125 GeV with the CMS experiment at the LHC*, *Phys.Lett.* **B716** (2012), [arXiv:1207.7235 \[hep-ex\]](https://arxiv.org/abs/1207.7235). 3
- [9] A. Pich, *The Standard Model of Electroweak Interactions*, [arXiv:1201.0537 \[hep-ph\]](https://arxiv.org/abs/1201.0537). 6, 7

- 838 [10] K. A. Olive at al. (Particle Data Group), *Review of Particle Physics*, *Chin.Phys. C* **38**(9)  
 839 (2014). 6
- 840 [11] J. Goldstone, A. Salam and S. Weinberg, *Broken Symmetries*, *Phys. Rev.* **127** (1962)  
 841 965–970. 8
- 842 [12] S. Weinberg, *Implications of Dynamical Symmetry Breaking*, *Phys. Rev.* **D19** (1976)  
 843 1277–1280. 10
- 844 [13] Super-Kamiokande Collaboration, Y. Fukuda et al., *Evidence for oscillation of*  
 845 *atmospheric neutrinos*, *Phys. Rev. Lett.* **81** (1998) 1562–1567, [arXiv:hep-ex/9807003](https://arxiv.org/abs/hep-ex/9807003)  
 846 [[hep-ex](#)]. 10
- 847 [14] SNO Collaboration, *Measurement of the Rate of  $\nu_e + d \rightarrow p + p + e^-$  Interactions*  
 848 *Produced by  ${}^8B$  Solar Neutrinos at the Sudbury Neutrino Observatory*, *Phys. Rev. Lett.*  
 849 **87** (2001). 10
- 850 [15] T. O. W. of the Nobel Prize.  
 851 [https://www.nobelprize.org/nobel\\_prizes/physics/laureates/2015/](https://www.nobelprize.org/nobel_prizes/physics/laureates/2015/). 10
- 852 [16] F. Jegerlehner, *The hierarchy problem of the electroweak Standard Model revisited*,  
 853 [arXiv:1305.6652](https://arxiv.org/abs/1305.6652) [[hep-ph](#)]. 12
- 854 [17] A. H. Chamseddine, R. Arnowitt, and P. Nath, *Locally Supersymmetric Grand*  
 855 *Unification*, *Phys. Rev. Lett.* **49** (1982) 970–974.  
 856 <https://link.aps.org/doi/10.1103/PhysRevLett.49.970>. 13
- 857 [18] A. Arbey, M. Battaglia, A. Djouadi, F. Mahmoudi, and J. Quevillon, *Implications of a*  
 858 *125 GeV Higgs for supersymmetric models*, *Physics Letters B* **708** no. 1, (2012) 162 – 169.  
 859 <http://www.sciencedirect.com/science/article/pii/S0370269312000810>. 13
- 860 [19] L. Randall and R. Sundrum, *Out of this world supersymmetry breaking*, *Nucl. Phys.*  
 861 **B557** (1999) 79–118, [arXiv:hep-th/9810155](https://arxiv.org/abs/hep-th/9810155) [[hep-th](#)]. 13
- 862 [20] G. F. Giudice, M. A. Luty, H. Murayama, and R. Rattazzi, *Gaugino mass without*  
 863 *singlets*, *JHEP* **12** (1998) 027, [arXiv:hep-ph/9810442](https://arxiv.org/abs/hep-ph/9810442) [[hep-ph](#)]. 13
- 864 [21] H. E. Haber and G. L. Kane, *The Search for Supersymmetry: Probing Physics Beyond the*  
 865 *Standard Model*, *Phys. Rept.* **117** (1985) 75–263. 14
- 866 [22] K. Hidaka and A. Bartl, *Impact of bosonic decays on the search for the lighter stop and*  
 867 *sbottom squarks*, *Phys. Lett.* **B501** (2001) 78–85, [arXiv:hep-ph/0012021](https://arxiv.org/abs/hep-ph/0012021) [[hep-ph](#)]. 14

- 868 [23] J.M. Jowett, M. Schaumann, R. Alemany, R. Bruce, M. Giovannozzi, P. Hermes, W.  
 869 Hofle, M. Lamont, T. Mertens, S. Redaelli, J. Uythoven, J. Wenninger, *The 2015*  
 870 *Heavy-Ion Run of the LHC*,  
 871 <http://accelconf.web.cern.ch/accelconf/ipac2016/papers/tupmw027.pdf>. 21
- 872 [24] O. S. Brüuning, P. Collier, P. Lebrun, S. Myers, R. Ostojic, J. Poole and P. Proudlock,  
 873 *LHC Design Report*, <https://cds.cern.ch/record/782076>. 22
- 874 [25] CMS Collaboration, *The CMS experiment at the CERN LHC*, Journal of  
 875 Instrumentation **3** no. 08, (2008) S08004.  
 876 <http://stacks.iop.org/1748-0221/3/i=08/a=S08004>. 22
- 877 [26] LHCb Collaboration, et. al, *The LHCb Detector at the LHC*, **JINST** (2008). 22
- 878 [27] ALICE Collaboration, *The ALICE experiment at the CERN LHC*, Journal of  
 879 Instrumentation **3** no. 08, (2008) S08002.  
 880 <http://stacks.iop.org/1748-0221/3/i=08/a=S08002>. 22
- 881 [28] A. Yamamoto, Y. Makida, R. Ruber, Y. Doi, T. Haruyama, F. Haug, H. ten Kate,  
 882 M. Kawai, T. Kondo, Y. Kondo, J. Metselaar, S. Mizumaki, G. Olesen, O. Pavlov,  
 883 S. Ravat, E. Sbrissa, K. Tanaka, T. Taylor, and H. Yamaoka, *The ATLAS central*  
 884 *solenoid*, **Nuclear Instruments and Methods in Physics Research Section A:**  
 885 **Accelerators, Spectrometers, Detectors and Associated Equipment** **584** no. 1, (2008)  
 886 53 – 74.  
 887 <http://www.sciencedirect.com/science/article/pii/S0168900207020414>. 24,  
 888 25
- 889 [29] ATLAS Collaboration, *The ATLAS Inner Detector commissioning and calibration*, **Eur.**  
 890 **Phys. JC** **70**, [arXiv:1004.5293](https://arxiv.org/abs/1004.5293). 25
- 891 [30] ATLAS Collaboration, *ATLAS Insertable B-Layer Technical Design Report*,  
 892 <https://cds.cern.ch/record/1291633>. 26
- 893 [31] G. A. et al., *ATLAS pixel detector electronics and sensors*, Journal of Instrumentation **3**  
 894 no. 07, (2008) P07007. <http://stacks.iop.org/1748-0221/3/i=07/a=P07007>. 27
- 895 [32] A. Bingül, *The ATLAS TRT and its Performance at LHC*, Journal of Physics:  
 896 Conference Series **347** no. 1, (2012) 012025.  
 897 <http://iopscience.iop.org/article/10.1088/1742-6596/347/1/012025/meta>.  
 898 27

- 
- 899 [33] ATLAS Collaboration, *ATLAS liquid-argon calorimeter: Technical Design Report.*,  
900 <https://cds.cern.ch/record/331061>. 29
- 901 [34] ATLAS Collaboration, *ATLAS muon spectrometer: Technical design report.*,  
902 <https://cds.cern.ch/record/331068>. 29
- 903 [35] ATLAS Collaboration, *Fast TracKer (FTK) Technical Design Report.*,  
904 <https://cds.cern.ch/record/1552953>. 31
- 905 [36] E. Simoni, *The Topological Processor for the future ATLAS Level-1 Trigger: from design to*  
906 *commissioning*, [arXiv:1406.4316](https://arxiv.org/abs/1406.4316). 32